Pinned Balseiro-Falicov model of tunneling and photoemission in the cuprates

R. S. Markiewicz and C. Kusko*
Department of Physics and Barnett Institute, Northeastern University, Boston, Massachusetts 02115

V. Kidambi
Department of Physics, Northeastern University, Boston, Massachusetts 02115

(Received 25 June 1998)

The smooth evolution of the tunneling gap of $Bi_2Sr_2CaCu_2O_8$ with doping from a pseudogap state in the underdoped cuprates to a superconducting state at optimal and overdoping, has been interpreted as evidence that the pseudogap must be due to precursor pairing. We suggest an alternative explanation, that the smoothness reflects a hidden SO(N) instability group near the $(\pi,0)$ points of the Brillouin zone (with $N=3,\ 4,\ 5$, or 6). Because of this group structure, the pseudogap could actually be due to any of a number of nesting instabilities, including charge or spin density waves or more exotic phases. We present a detailed analysis of this competition for one particular model: the pinned Balseiro-Falicov model of competing charge density wave and (s-wave) superconductivity. We show that most of the anomalous features of both tunneling and photoemission follow naturally from the model, including the smooth crossover, the general shape of the pseudogap phase diagram, the shrinking Fermi surface of the pseudogap phase, and the asymmetry of the tunneling gap away from optimal doping. Below T_c, the sharp peak at Δ_1 and the dip seen in the tunneling and photoemission near $2\Delta_1$ cannot be described in detail by this model, but we suggest a simple generalization to account for inhomogeneity, which does provide an adequate description. We show that it should be possible, with a combination of photoemission and tunneling, to demonstrate the extent of pinning of the Fermi level to the Van Hove singularity. A preliminary analysis of the data suggests pinning in the underdoped, but not in the overdoped regime. [S0163-1829(99)03325-1]

I. INTRODUCTION

A. Precursor pairing?

Recent photoemission[1–3] and tunneling[4–9] studies have provided a picture of unparalleled detail of the opening of the pseudogap in the underdoped cuprates. The most remarkable feature is that the pseudogap evolves smoothly into the superconducting gap as doping increases. This has led a number of researchers to conclude that the pseudogap must itself be related to superconductivity: that it represents a form of short-range superconducting order, or precursor pairing.[10] It is the purpose of the present paper to show that this is not a foregone conclusion: there is an alternative interpretation (better: class of interpretations) in which the pseudogap represents a *competing* ordered state. In this case, the apparently smooth evolution is due to an *underlying symmetry of the instabilities* of the problem — a manifestation of an SO(N) group, with $N=3$,[11] 4,[12] 5,[13] or 6.[14]

For such an interpretation to hold, certain very strict conditions must be met. Specifically, there must be a Van Hove nesting,[15] with the Van Hove singularity (VHS) pinned close to the Fermi level ϵ_F over an extended doping range. This prediction is now within the realm of experimental test, and a preliminary analysis (Sec. III C) of the existing data seems to confirm the pinning.

To describe the competing order parameters, we analyze a simple generic model, the pinned Balseiro-Falicov[16] (BF) model. Within this model, the total gap has a maximum at $(\pi,0)$ in the Brillouin zone, given by

$$\Delta_t=\sqrt{\Delta_k^2+G_k^2}, \tag{1}$$

where Δ_k is an (s-wave) superconducting gap and G_k a charge-density wave (CDW) gap, defined below. This is exactly the form proposed phenomenologically by Loram *et al.*,[17] and it immediately explains the smooth evolution of the gap with doping: there is a single gap [at $(\pi,0)$] at all dopings, even though the system changes over from CDW near half filling to superconductor near optimal doping. The form of Eq. (1) immediately follows from the SO(3) group structure. It is in principle possible to disentangle the nature of the gaps from their behavior away from $(\pi,0)$, although this involves symmetry breaking terms, and hence is considerably more model dependent. The SO(N) structure also suggests that the pinned BF (pBF) model should provide a good approximate representation for a wide range of competing phases — in particular the pseudogap phase may also be an antiferromagnetic phase or a flux phase (which is a form of dynamic CDW), or indeed a striped phase which is a combination of two of these phases.

B. Van Hove pinning

In the generalized Van Hove scenario,[18] there are two separate phenomena which contribute to Van Hove pinning. First, as part of the Mott-Hubbard transition, strong Hubbard-U correlation effects renormalize Cu-O hopping t to zero at half filling, leaving a residual energy dispersion associated with exchange J. In the absence of correlation effects, the ''bare'' VHS would fall at a finite hole doping fixed by the band parameters (t' in the $tt'J$ model) — this doping will be close to, but not necessarily the same as optimal doping. However, since second (Cu) neighbor ex-

change is expected to be small, the exchange bands have the simple dispersion $J(c_x+c_y)$, where $c_i=\cos k_i a$. Hence, at half filling, the Fermi level approximately coincides with the VHS. This phase can be further stabilized by Van Hove nesting, which opens up a large gap in the dispersion near $(\pi,0)$. A good fit to the dispersion in the related insulating compound[19] $Sr_2CuO_2Cl_2$ (SCOC) can be found[20–22] by assuming that the nesting is associated with a flux phase.[23]

With doping, t is gradually restored, producing a behavior which cannot be described by a rigid band filling model. At first, the VHS shifts faster than the Fermi level, so the VHS lies *below* the Fermi level, but very close to it. Gradually, t saturates, the VHS stops shifting (usually close to its bare value), and at some finite doping x_c the Fermi level crosses this new VHS. Thus, the Fermi level coincides with the VHS *twice*: at half filling and near the bare VHS, and remains anomalously close at intermediate dopings. Since its initial discovery,[24] this correlation induced pinning has been confirmed by a number of calculations.[25]

But even stronger pinning is possible. Near x_c, the energy can be significantly lowered by a second nesting instability. Assuming this second instability to be charge-density wave related, a self-consistent three-band slave boson calculation demonstrated that this model can lead to two free energy minima, one at half filling and the other at x_c.[22] This results in striped phases, with each phase pinned near a VHS: the magnetic stripes near the J-dominated VHS near half filling, and the charged stripes near the t-dominated VHS at x_c. Since the stripes are nanoscale (due to long-ranged Coulomb repulsion), the system evolves rather smoothly with doping, with the Fermi level remaining even more strongly pinned to the VHS at all dopings.

While the above model is in good agreement with experiments on both the pseudogaps and the striped phases,[26] the identification of the specific nesting instability phases is less secure. This is because the nesting and pairing instabilities of the Van Hove scenario form two six-dimensional superspins of a group SO(6) (Ref. 14) so the issue of which phase is the most unstable depends sensitively upon secondary parameters which are not well known. The various possibilities include the antiferromagnetic and d-wave superconducting instabilities of Zhang's SO(5),[13] as well as CDW's, flux phases, and a more exotic spin current phase.[27] (Two-leg ladders have an even larger assortment of instabilities to choose from.[28]) It is difficult to incorporate the details of this phase separated regime rigorously into calculations of the ARPES and tunneling spectra.

Nevertheless, a remarkably simple picture of the pseudogap (VH nesting) phase diagram can be developed via a simple ansatz for the pinned striped phases. A one band model is assumed

$$\epsilon_k=-2t(c_x+c_y)-4t'c_xc_y \tag{2}$$

(with $c_i=\cos k_i a$), and the second neighbor hopping is adjusted with doping to pin the VHS to the Fermi level over a doping range from half filling $x=0$ to a doping x_c. Approximately,[18]

$$\tau=\frac{2t'}{t}=-1.04\tanh 2.4x. \tag{3}$$

Within this model the striped phase is represented by a single nesting instability which splits the band dispersion at $(\pi,0)$. Such a model was initially introduced (without the pinning) by Balseiro and Falicov[16] to study the competition between CDW's and s-wave superconductivity. We have employed this pinned Balseiro-Falicov (pBF) model in previous pseudogap studies[29–31] and will continue to use it here. (It must be stressed that we do not employ the CDW's to mimic the spatial pattern of the stripes, but rather to reproduce the Fermi level pinning.) We are currently generalizing the model to include d-wave superconductivity and a variety of other nesting instabilities. In the present version, there are electron-phonon coupling energies λ_G associated with CDW's, and λ_Δ with superconductivity, which may or may not be equal. The gap equations are solved self-consistently, with free parameters t, x_c, the λ_i's, and $\omega_{\rm ph}$, a bosonic cutoff frequency. There is relatively little data in the overdoped regime, so we choose a simple model: for $x>x_c$, the band parameters cease evolving, and the additional holes just rigidly fill the band, shifting the Fermi level away from the VHS. This simple picture appears capable of describing the overdoped regime in both $YBa_2Cu_3O_{7-\delta}$ (YBCO), where the pseudogap vanishes close to optimal doping[32] and $La_{2-x}Sr_xCuO_4$ (LSCO), where the pseudogap appears to persist well into the overdoped regime.[33] However, a more complicated behavior, including a second range of two-phase coexistence (Secs. 11.6 and 11.7 of Ref. 18), is not ruled out.

Within this picture, there is a natural doping dependence associated with the competition between nesting and pairing instabilities. At half filling, $t'=0$, the perfect nesting overwhelms the pairing instability, leading to a pure nesting instability. As t' increases with doping (to maintain the VH pinning), the nesting gets worse, while pairing is less affected (it is actually enhanced, Sec. II B). This leads to a crossover to a pairing instability as a function of doping. Since nesting does not gap the full Fermi surface (when t' is large enough), superconductivity can appear at a lower temperature, with a T_c which increases with doping. As long as the VHS remains pinned to the Fermi level and the electron-phonon coupling remains doping independent, the nesting T_n will decrease with doping x while the superconducting T_c will increase. At some point, the two transitions would cross. However, at this point T_n will be rapidly suppressed to zero, since superconductivity gaps essentially the full Fermi surface (the small residual Fermi surface for a d-wave gap could only sustain a nesting instability at a much lower T). While exactly this behavior is found in YBCO, in LSCO, and probably $Bi_2Sr_2CaCu_2O_8$ (Bi-2212) as well the pseudogap persists into the overdoped regime. This behavior can be modelled by having the strength of the bosonic pairing decrease with increasing x.

Since nesting splits the VHS degeneracy, we introduce some notation to clarify the following discussions. The lower VHS (VHL) is the VHS shifted below the Fermi level, at energy E_L, and hence visible in photoemission. The upper VHS (VHU) is shifted to E_U, above the Fermi level, and hence can only be seen in tunneling (or inverse photoemission). In conventional plots of tunneling spectra, VHL appears at negative voltages, in the electron extraction mode, and VHU at positive voltages. The Van Hove centroid (VHC) is the average position of these two features E_C

$=(E_U+E_L)/2$ — it is the position at which the single, unsplit VHS would fall at high temperatures, well above the pseudogap transition.

In terms of these features, the photoemission gap is $\Delta_{\rm PE}=\epsilon_F-E_L$. We will show (Fig. 5 below) that the tunneling gap is $\Delta_{\rm TU}=(E_U-E_L)/2$. In this case, the pinning of the Fermi level at the VHC, $\epsilon_F\simeq E_C$, can be rewritten in terms of measurable quantities as $\Delta_{\rm TU}=\Delta_{\rm PE}$. In Sec. III C, below, we will demonstrate that this relationship appears to be satisfied in the underdoped regime.

II. STRIPED PHASES AND PSEUDOGAP

A. Phase diagram of pinned BF model

For completeness, we recall the energy dispersion and the gap equations of the BF model. In terms of the four-component wave vector $\Psi_{\vec{k}}^{\dagger}=(\psi_{\vec{k}}^{\dagger},\psi_{\vec{k}+\vec{Q}}^{\dagger},\psi_{-\vec{k}},\psi_{-(\vec{k}+\vec{Q})})$, the mean field BF Hamiltonian tensor is

$$H_{\rm BF}=\begin{pmatrix} \epsilon_{\vec{k}}-\epsilon_F & -G_{\vec{k}} & -\Delta_{\vec{k}} & 0 \\ -G_{\vec{k}} & \epsilon_{\vec{k}+\vec{Q}}-\epsilon_F & 0 & -\Delta_{\vec{k}+\vec{Q}} \\ -\Delta_{\vec{k}} & 0 & -\epsilon_{\vec{k}}+\epsilon_F & G_{\vec{k}} \\ 0 & -\Delta_{\vec{k}+\vec{Q}} & G_{\vec{k}} & -\epsilon_{\vec{k}+\vec{q}}+\epsilon_F \end{pmatrix}. \tag{4}$$

In terms of a function

$$\Theta_{\vec{k}}=\begin{cases} 1 & \text{if } |\epsilon_{\vec{k}}-\epsilon_F|<\hbar\omega_{\rm ph}, \\ 0 & \text{otherwise,} \end{cases} \tag{5}$$

the gap functions are $\Delta_{\vec{k}}=\Delta\Theta_{\vec{k}}$ for superconductivity, and $G_{\vec{k}}=G_0+G_1\Theta_{\vec{k}}\Theta_{\vec{k}+\vec{Q}}$ for the CDW. [This latter result generalizes Balseiro and Falicov's Eq. (3.3), which is valid for $t'=0$.] The energy eigenvalues are $E_{\pm,k}$ and their negatives, with

$$E_{\pm,k}^2=\frac{1}{2}(E_k^2+E_{k+Q}^2+2G_k^2\pm\hat{E}_k^2), \tag{6}$$

$E_k^2=\epsilon_k^2+\Delta_k^2$, $\hat{E}_k^4=(E_k^2-E_{k+Q}^2)^2+4G_k^2\tilde{E}_k^2$, $\tilde{E}_k^2=\epsilon_{k+}^2+(\Delta_k-\Delta_{k+Q})^2$, $\epsilon_{k\pm}=\epsilon_k\pm\epsilon_{k+Q}$, and the nesting vector $Q=(\pi,\pi)$. If the magnitudes of the (attractive) phonon-induced electron-electron interaction energies are λ_Δ and λ_G, then the gap equations are

$$\Delta=\lambda_\Delta\Delta\Sigma_{\vec{k}}\frac{\Theta_{\vec{k}}}{E_{+,k}^2-E_{-,k}^2} \times\left(\frac{E_{+,k}^2-\epsilon_{\vec{k}+\vec{Q}}^2-\Theta_{\vec{k}+\vec{Q}}[\Delta^2+G_{\vec{k}}^2]}{2E_{+,k}}\tanh\frac{E_{+,k}}{2k_BT}-\frac{E_{-,k}^2-\epsilon_{\vec{k}+\vec{Q}}^2-\Theta_{\vec{k}+\vec{Q}}[\Delta^2+G_{\vec{k}}^2]}{2E_{-,k}}\tanh\frac{E_{-,k}}{2k_BT}\right), \tag{7}$$

$$G_i=\lambda_G\Sigma_{\vec{k}}\frac{\Theta_i G_{\vec{k}}}{E_{+,k}^2-E_{-,k}^2}\left(\frac{E_{+,k}^2+\epsilon_{\vec{k}}\epsilon_{\vec{k}+\vec{Q}}-\Delta_{\vec{k}}^2-G_{\vec{k}}^2}{2E_{+,k}}\tanh\frac{E_{+,k}}{2k_BT}-\frac{E_{-,k}^2+\epsilon_{\vec{k}}\epsilon_{\vec{k}+\vec{Q}}-\Delta_{\vec{k}}^2-G_{\vec{k}}^2}{2E_{-,k}}\tanh\frac{E_{-,k}}{2k_BT}\right), \tag{8}$$

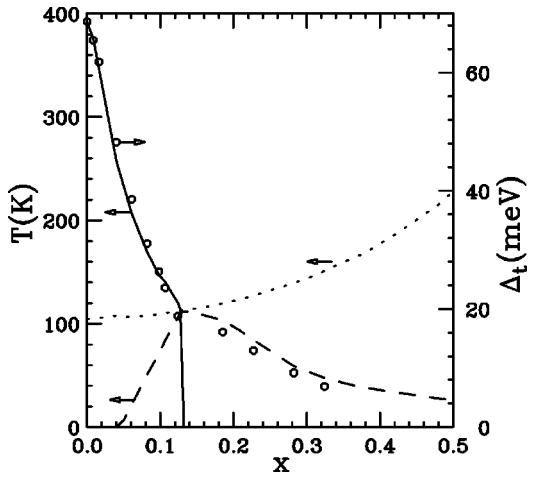

FIG. 1. Phase diagram of pinned Balseiro-Falicov model. Circles=net tunneling gap Δ_t; solid line=CDW transition temperature T_p; dashed line=superconducting transition T_c; dotted line=T_c in absence of CDW, $x_c>0.5$.

with $\Theta_0=\Theta_{\vec{k}}\Theta_{\vec{k}+\vec{Q}}$, $\Theta_1=1$. A similar model[34] has recently been applied to analyze the photoemission associated with a pure CDW phase.

In the pinned BF (pBF) model, the Fermi level is pinned to the VHC, via Eq. (3), for doping x between half filling ($x=0$) and some critical doping x_c, while for $x>x_c$, the curvature is fixed at $t'=t'(x_c)$, while the Fermi level shifts off of the VHC in a rigid band filling.

For fixed values of the parameters t, x_c, λ_i, and phonon cutoff $\omega_{\rm ph}$, the pseudogap phase diagrams are derived by solving Eqs. (6)–(8) self-consistently. For Fig. 1, the parameter values are chosen as $t=\lambda_\Delta=\lambda_G=0.25$ eV, $\omega_{\rm ph}=45$ meV, and $x_c=0.123$. At half filling, perfect nesting wins out over superconductivity, but with doping the nesting becomes poorer, while superconductivity is enhanced, leading to a crossover. As soon as the superconducting T_c is larger than $T_{\rm CDW}$, $T_{\rm CDW}$ is rapidly suppressed to zero. The dotted line in Fig. 1 shows how T_c would evolve in the absence of the CDW, if the Fermi level remained pinned to the VHC over the full doping range ($x_c>0.5$). A typical temperature dependence of the resulting gaps is illustrated in Fig. 2, for $x=0.1$. Note that Δ_t, Eq. (1), is found self-consistently to evolve smoothly with temperature; this implies that G_k must actually decrease when superconductivity appears, $\Delta_k\neq 0$.

To reproduce the phase diagram of YBCO, the crossover must arise close to x_c, as in Fig. 1, while in LSCO it falls well after x_c, Fig. 3. The phase diagram of LSCO can be modelled by choosing $\lambda_G\neq\lambda_\Delta$, and letting the latter vary with doping, Fig. 3. Here, λ_Δ is adjusted at each doping to reproduce the known $T_c(x)$. The doping dependence of λ_Δ (inset, Fig. 3) is weak until well in the overdoped regime, $x>0.2$. Possible significance of this doping dependence is discussed in Sec. V D.

One feature of Fig. 3 should be noted. In LSCO the pseudogap appears in some experiments to persist into the overdoped regime,[33,35] while other experiments find a striking crossover in properties at optimal doping.[36–38] In the thermodynamic experiments,[35] the pseudogap appears to be closing linearly with doping, but then has a *break in slope at*

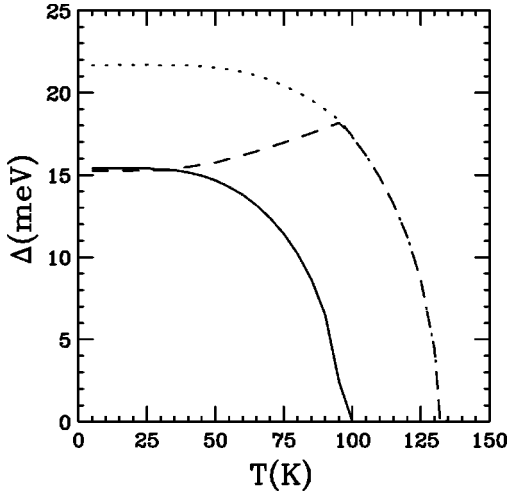

FIG. 2. Evolution of gaps in pinned Balseiro-Falicov model. Solid line=superconducting gap Δ_k; dashed line=CDW gap $G_k = G_0 + G_1$; dotted line=net gap, Δ_t, Eq. (1). Parameters correspond to Fig 1, $x = 0.1$.

optimal doping, and falls off more slowly at larger doping. Figure 3 mimics this behavior: the Fermi level is pinned at the VHC until optimal doping $x_c = 0.16$, and then depins. Despite the fact that the Fermi level now shifts with doping away from the VHC, the CDW instability is strong enough that the CDW phase persists out to $x = 0.27$, at which point it becomes unstable (discontinuously). Such behavior is only possible because the superconducting transition is suppressed far below T_p.

The pBF model is a two-dimensional (2D) mean field theory. In a more accurate three-dimensional calculation,[39] the transition temperatures in the above phase diagram will be replaced by crossover temperatures at which 2D fluctuations become strong — i.e., temperatures at which a pseudogap opens. When interlayer coupling becomes strong

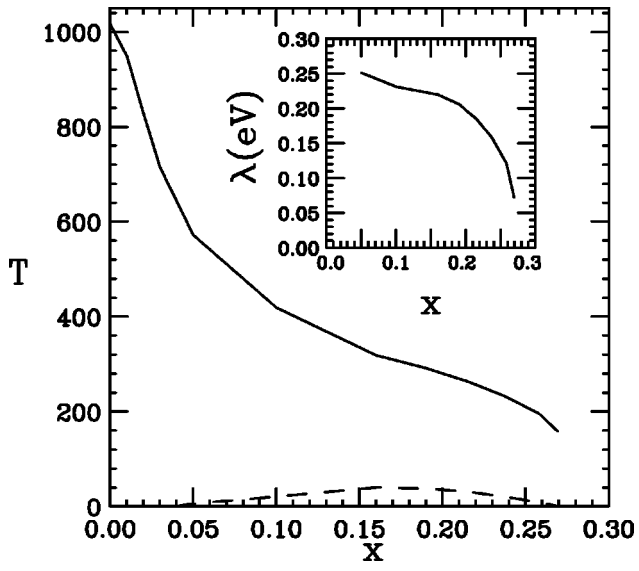

FIG. 3. Model pseudogap phase diagram for LSCO. Parameters $x_c = 0.16$, $\lambda_G = 0.6$ eV, with doping dependent λ_Δ (inset). Solid line=CDW transition temperature T_d; dashed line=superconducting transition T_c.

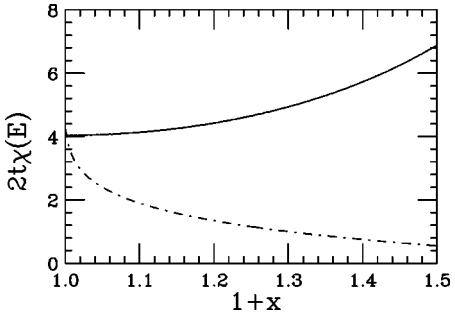

FIG. 4. Susceptibilities χ_Q (dotdashed line) and χ_0 (solid line) vs band filling $1+x$ for Eq. (2) with $4t' = E_F$ (pinned VHC).

enough, a real three-dimensional order, with true energy gaps, can develop. This is discussed further in Sec. V C.

A (weak-coupling) limitation of the BF model is the discontinuous change in Δ and G_1 when the energy crosses $\omega_{\rm ph}$. When this feature becomes prominent in the dispersion, the BF results must be considered as only a qualitative indication of the results of a proper strong coupling calculation.

B. SO(6)

Whereas the above discussion has been in terms of a particular competition — between a CDW and an *s*-wave superconductor, the results are indicative of a much more general situation. That is because the VHS instability has an underlying SO(8) spectrum generating algebra (SGA), with associated SO(6) instability group.[14] There is actually a pair of six-dimensional ''superspins,'' which consist of various nesting or pairing instabilities of the VHS. Nesting (pairing) operators are those instability operators which do (do not) commute with the number operator Q.

The distinction between an instability group and a symmetry group should be stressed. An SGA (Ref. 40) allows one to find all of the eigenfunctions of a Hamiltonian — in particular, the allowable ground states, or instabilities. Thus, the instability group is a generalization of the *g*-ology model of a one-dimensional metal,[41] and allows phase diagrams to be constructed as a function of interaction parameters. For special values of the parameters, there may be a degeneracy, leading to an interesting symmetry group, but this is more the exception than the rule. Here we will show that the SO(6) instability group can provide valuable information about the pseudogap, *even though the BF model does not possess SO(6) [or even SO(3)] symmetry*.

Within SO(8), the instabilities depend on two factors, the bare susceptibilities $\chi_0(\vec{q},\omega)$, and the interaction parameters G (e.g., the λ's of the pBF model). The group structure is manifest in the χ_0's: at half filling, with $t' = 0$, all susceptibilities are degenerate. Doping, or setting $t' \neq 0$ breaks the degeneracy, but only into two classes, $\chi_0 = \chi_0(\vec{q} = 0,0)$ for the pairing instabilities and $\chi_Q = \chi_0(\vec{q} = \vec{Q},0)$ for the nesting instabilities, Fig. 4.[14] While the actual instabilities observed are controlled by the G values, if the G's happen to be only weakly dependent on doping, then *the phase diagram has a characteristic form, depending only on the susceptibility*.

A comparison of Fig. 1 with Fig. 4 shows the close connection between the phase diagram and the underlying susceptibilities, the solid line in Fig. 1 (pseudogap phase) re-

sembling the nesting susceptibility (a larger susceptibility corresponding to a higher transition temperature), while the pairing susceptibility resembles the superconducting phase (dotted lines in Fig. 1). In general, a finite t' reduces nesting while increasing pairing. This *generic* SO(6) feature strongly suggests that the pseudogap is associated with a nesting instability.

The phase diagram of Fig. 1 shows additional evidence for the underlying SO(N) nature of the VHS: (a) despite a crossover from CDW to superconducting, the evolution of the total gap Δ_t and transition temperature T_t with doping is extremely smooth; indeed, the gap ratio $2\Delta(0)/k_BT_c \simeq 4.1$ is nearly independent of doping. (b) The total gap is given by a vector addition, Eq. (1).

Note finally that just these features (a) and (b) have been taken as evidence that the pseudogap must itself be related to superconductivity as a form of precursor pairing. Instead, we find that the phase diagram of Fig. 1 should look fairly similar for *any* competition between a nesting and a pairing instability — e.g., either CDW vs *s*-wave superconductivity or SDW vs *d*-wave superconductivity. The actual phases observed will depend on the interaction parameters, and may vary with doping. Note, however, that the pseudogap is clearly a nesting, and not a pairing instability. Hence, it seems unlikely that the experimental pseudogap could be associated with superconducting fluctuations.

Experimentally, there is evidence for striped phases[26] at intermediate dopings. In SO(5), these stripes can be interpreted as a combination of magnetic and superconducting stripes. However, in this case it is not clear how to interpret the 1/8 anomaly ($x=1/8$) where the stripes show long range order but there is no superconductivity. It seems more likely that superconductivity competes with the stripes, and that the stripes arise from a competition between two nesting instabilities, the flux phase at half filling and a CDW near x_c.[22] It is important to recognize that the flux phase does not involve the electron spins — the magnetic moments are orbital. Hence, the phase is best understood as a *dynamic CDW phase* (compare Refs. 42 and 43), so a model which approximates the pseudogap by a CDW ansatz (such as the pBF model) should provide a quite reasonable first approximation.

C. Tunneling spectra

Under certain special conditions, both the tunneling and photoemission can reveal very direct information about the spectral function of the interacting electrons. The quasiparticle tunneling current can be written[44]

$$I = 2e\Sigma_{\vec{k}\vec{p}}|T_{\vec{k}\vec{p}}|^2 \int_{-\infty}^{\infty} \frac{d\epsilon}{2\pi} A_R(\vec{k},\epsilon) A_L(\vec{p},\epsilon+eV) \times [n_F(\epsilon) - n_F(\epsilon+eV)], \tag{9}$$

where $T_{\vec{k}\vec{p}}$ is the tunneling matrix element, A_i is the appropriate spectral function in the metal on the left (L) and right (R) of the tunneling junction. If the tunneling matrix element is considered to be constant, independent of $\vec{k}$ and $\vec{p}$, it can be taken out of the integral, yielding

$$I = 2eT^2 \int_{-\infty}^{\infty} \frac{d\epsilon}{2\pi} N_R(\epsilon) N_L(\epsilon+eV)[n_F(\epsilon) - n_F(\epsilon+eV)], \tag{10}$$

with N_i the appropriate DOS. For an NIS junction, taking N_L to be energy independent, the tunneling conductance is

$$G = \frac{\partial I}{\partial V} = \frac{e^2T^2}{\pi} N_L N_R(-eV). \tag{11}$$

The conventional wisdom[45] is that tunneling is not sensitive to the density of states (DOS): the explicit factor of DOS in Eq. (9) is cancelled by $T^2 \propto v_F$, the Fermi velocity. However, Wei, *et al.*[46] have shown that this cancellation breaks down in the presence of strong anisotropy. In particular, *tunneling along the c direction into a two-dimensional metal directly measures the in-plane DOS* (at least in the thin junction limit). Hence, in accord with Eq. (11), the tunneling conductance is proportional to the tunneling DOS. This result is the basis for the present analysis. For three-dimensional materials, there have been previous proposals that the VHS's should show up in tunneling,[47] and the tunneling spectra of CDW superconductors have been analyzed.[48]

The tunneling and photoemission are derived from the spectral function of the model

$$A(k,\omega) = 2\pi\Sigma_{i=\pm}[u_{i,k}^2 \delta(\omega - E_{i,k}) + v_{i,k}^2 \delta(\omega + E_{i,k})], \tag{12}$$

with eigenenergies given by Eq. (6), and coherence factors

$$u_{\pm,k} = u_{\pm,0}\cos(\phi + \phi_{\mp}), \tag{13}$$

$v_{\pm,k}^2 = u_{\pm,0}^2 - u_{\pm,k}^2$,

$$u_{+,0}^2 = 1 - u_{-,0}^2 = \frac{1}{2}\left(1 + \frac{E_k^2 - E_{k+Q}^2}{\hat{E}_k^2}\right), \tag{14}$$

$$\cos^2\phi = \frac{1}{2}\left(1 + \frac{\epsilon_k + \epsilon_{k+Q}}{\tilde{E}_k}\right), \tag{15}$$

$$\cos^2\phi_{\pm} = \frac{1}{2}\left(1 + \left[\frac{E_{\pm,k}^2 + \epsilon_k\epsilon_{k+Q} - \Delta_k\Delta_{k+Q} + G_k^2}{\tilde{E}_k E_{\pm,k}}\right]\right), \tag{16}$$

$$\sin 2\phi = \frac{\Delta_k - \Delta_{k+Q}}{\tilde{E}_k}, \tag{17}$$

$$\sin 2\phi_{\pm} = \frac{\Delta_k\epsilon_{k+Q} + \Delta_{k+Q}\epsilon_k}{E_{\pm,k}\tilde{E}_k}. \tag{18}$$

In deriving the spectral function, it is convenient to use the group theoretical techniques of spectrum-generating algebras.[14] For a pure CDW ($\Delta_k = 0$), the spectral function simplifies to

$$A(k,\omega) = 2\pi[u_k^2 \delta(\omega - E_{k+}) + v_k^2 \delta(\omega - E_{k-})], \tag{19}$$

with $u_k^2 = 1 - v_k^2 = (1 + \epsilon_{k-}/\tilde{E}_k')/2$,

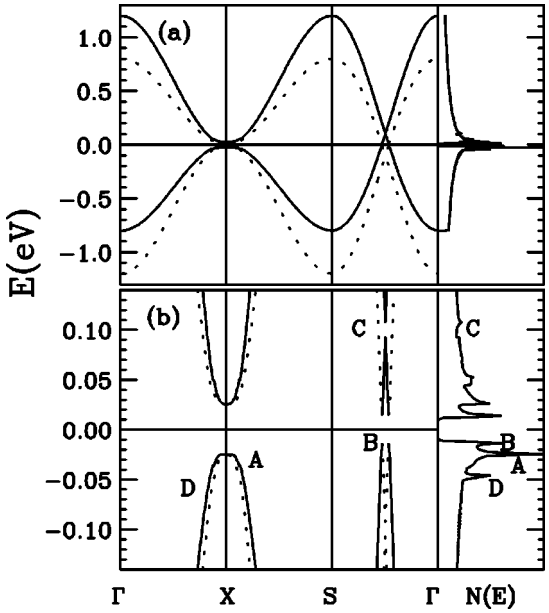

FIG. 5. Energy dispersion for data of Fig. 1, with $\tau=-0.2$, $T=10$ K. Right=tunneling DOS. (a) full dispersion; (b) blow-up of region near ϵ_F.

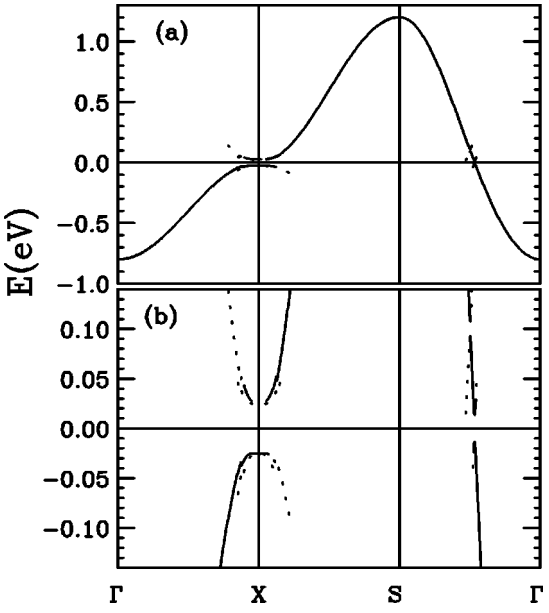

FIG. 6. Replot of energy dispersion of Fig. 5, illustrating spectral weight. Coherence factor $\geqslant 0.6$: solid lines; between 0.1 and 0.6: dashed lines; between 0.001 and 0.1: dotted lines.

$$E_{k\pm}=(\epsilon_{k+}\pm\tilde{E}'_k)/2, \tag{20}$$

and $\tilde{E}'_k=\sqrt{\epsilon_{k-}^2+4G_k^2}$.

Figure 5 shows the energy dispersion for a combined CDW-superconductor (left) and the associated DOS (right). Part (a) shows the full dispersion, while (b) is a blow-up of the region near the Fermi level. There are four bands; the CDW order folds the M point of the Brillouin zone into the Γ point, while superconductivity folds both of these bands around the Fermi level (dotted lines). However, these ghost bands carry little spectral weight (coherence factor $\ll 1$) except very near the Fermi level — note that there is no indication of the tops or bottoms of the dotted lines in the DOS. Figure 6 replots the dispersion, giving an indication of the spectral weight. See further Fig. 10, below.

A close look at the region near the Fermi level, Fig. 5(b), reveals that structure in the tunneling DOS is directly related to features in the dispersion of the gapped bands. Thus, peak A is associated with the dispersion at $(\pi,0)$ — the VHS peak split by the combined CDW-superconducting gap. Peak B is due to the superconducting gap away from $(\pi,0)$ — particularly near $(\pi/2,\pi/2)$. Accordingly, it will be considerably less prominent for a d-wave superconductor, where the gap vanishes at $(\pi/2,\pi/2)$. Feature C is associated with the CDW gap G_k near $(\pi/2,\pi/2)$. As discussed in Ref. 22, Equation (20) can be rewritten as

$$E_{k\pm}=-4t'c_xc_y\pm\sqrt{4t^2(c_x+c_y)^2+G_k^2}, \tag{21}$$

showing that the CDW gap is fixed to the VHS, but not to the Fermi level, so that at $\vec{k}$ points away from $(\pi,0)$ there can be two gaps at different energies. Feature C is further discussed in Ref. 34. Whether this is only a weak-coupling effect that would be washed out in a strong-coupling theory remains to be seen. Finally, feature D is associated with the phonon-related discontinuities in the dispersion at $\omega_{\rm ph}$.

The appearance of two gaplike features in the tunneling spectrum is not necessarily a consequence of two competing order parameters, but of gap anisotropy. Indeed, for a pure (generalized) s-wave superconductor, there will be two peaks in the tunneling DOS whenever the gap is anisotropic, as long as the minimum gap is nonzero. Moreover, even for a pure d-wave superconductor, there can be two gaplike features if the VHS is not at the Fermi level, Fig. 10.

D. Line broadening

In the one-dimensional CDW, the principal source of line broadening above the Peierls transition is CDW fluctuations.[49–51] The phonon propagator diverges at the transition

$$D(q)\simeq\frac{1}{\xi^{-2}+|\vec{q}-\vec{Q}|^2}, \tag{22}$$

with $\xi^{-2}\propto(T-T_p)$. For the two-dimensional Van Hove problem, a similar form holds[39] with $T_p=0$ in the absence of interlayer coupling. This results in an intrinsic broadening $\Gamma=v_F/\xi\propto\sqrt{T}$.

In the superconductor, a true long-range ordered state is possible, with a real gap at the Fermi surface leading to a considerably reduced Γ. Such a reduced scattering has been observed in a number of transport properties, as well as in the photoemission spectrum. However, the scattering should be restored at high frequencies, when the CDW fluctuations can break a pair. On analogy with the results of Coffey and Coffey,[52] we assume that the crossover will fall near $2\Delta_k$. (Strictly speaking, the crossover should be at $3\Delta_k$ for an s-wave superconductor.)

III. COMPARISON TO EXPERIMENT

A. Experimental situation

Both photoemission and tunneling measurements of the pseudogap have been largely restricted to Bi-2212. While the general features of the spectra are reasonably well understood, there are still differences in detail. In this subsection, we summarize a number of unresolved issues.

(a) In optimally doped and lightly underdoped Bi-2212, photoemission detects a significant rearrangement of spectral weight in the superconducting state. The low-temperature ($T<T_c$) spectra are generally characterized by three features: a sharp quasiparticle *peak* Δ_1 separated from the Fermi level by a small ($\sim 25-50$ meV) gap and a broad *hump* at much higher energies, Δ_2 separated by a well-defined *dip* at energy $\sim 2\Delta_1$. Above T_c, the peak and dip disappear, leaving a feature similar to the hump.

The dip feature is now widely interpreted as coupling to some form of collective mode, the exact nature of which is not well understood. The fact that it varies with doping, scaling as $2\Delta_1$ is puzzling. One possible interpretation is that it is related to electron-electron scattering. The broadening of the photoemission features is known to decrease dramatically just below T_c, and this decrease would be expected to fall off at frequencies much larger than the gap (at 3Δ for an *s*-wave superconductor, 2Δ for *d* wave). Such a result could be very useful in separating the superconducting gap from the pseudogap, but fits to this model have been unsuccessful in reproducing the dip amplitude. We will show (Sec. III E) that it is possible to get a large dip if there is significant spectral weight in the hump feature.

(b) The presence of the dip has led to some confusion on the doping dependence of ''the gap'': should one count Δ_1 or Δ_2. The latter choice was made by Marshall *et al.*[1] In their earlier work, the Argonne group used neither choice, but defined the gap in terms of the leading edge near ϵ_F. This feature should scale with the peak position of Δ_1, but be somewhat smaller. In their more recent work they have used the peak position Δ_1 for better comparison with tunneling studies. Our analysis suggests that this is a more appropriate choice, and we shall follow this latter usage. Our own belief is that, since the hump persists above T_c, Δ_2 is a proper candidate for the pseudogap. However, it is not always easy to extract this feature from the published literature. Fortunately, Ding[53] is now carrying out a careful study of both gaps.

Near optimal doping, $\Delta_1 \simeq \Delta_2$, so the literature uncertainty will not greatly affect our reconstructed phase diagram, Fig. 7, below. For stronger underdoping, the sharp peak and dip gradually wash out, while the hump shifts to higher energy. We find that this shift is clearly revealed in the doping dependence of T^*, the temperature onset of the pseudogap,[54] and that these data are consistent with the Stanford measurements of the hump data, suggesting that the photoemission provides a single pseudogap phase diagram. Moreover, this diagram is remarkably consistent with the pseudogap phase diagrams found for LSCO and YBCO on the basis of transport measurements.

(c) Tunneling is mainly sensitive to the sharp peak and dip feature in the superconducting state, and it is not always clear whether the hump feature is seen. However, some groups clearly do see structure above T_c.[6] One problem is that tunneling is very surface sensitive, and the BiO layer on the top surface has an insulating gap. However, consistency with the photoemission would suggest that a pseudogap should be present above T_c. Recently, Renner, *et al.*[55] have reported that the tunneling gap inside a vortex core resembles that found in the pseudogap above T_c.

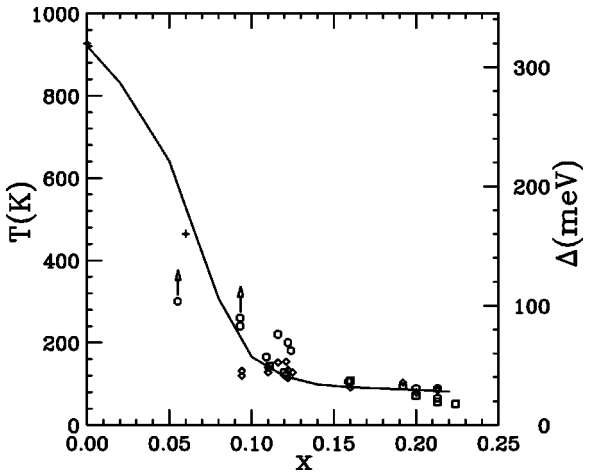

FIG. 7. Pseudogap phase diagram in Bi-2212 determined from photoemission and tunneling. Diamonds=photoemission gap (Ref. 54); +=photoemission gap (Refs. 1,19); circles=T^* measured from photoemission (Ref. 54); squares=tunneling gap (Ref. 8). Solid line=guide to the eye.

(d) There is a question about overdoping, with Renner *et al.*[6] detecting the pseudogap in overdoped samples, while photoemission studies[56] find a rapid collapse of the pseudogap in overdoped Bi-2212. It seems likely, however, that in LSCO the pseudogap persists well into the overdoped regime.[33]

(e) There is also some disagreement on the gap ratio $2\Delta(0)/k_BT^*$, with Oda *et al.*[4] reporting a value 4–5, whereas a value ~ 8 can be extracted from the data of Ding *et al.*[54]

B. Pseudogap phase diagram

Figure 7 summarizes the photoemission and tunneling data on the pseudogap in Bi-2212. Most of the photoemission data are taken from the Argonne group,[54] but the two lowest dopings are from the Stanford group,[1] and from the insulating phase, $Sr_2CuO_2Cl_2$.[19] Since there has been disagreement on how to determine the pseudogap peak position, it is important to note that the Argonne data are consistent with a large increase in T^* (open circles) at low doping. This pseudogap determined from *photoemission* in Bi-2212 is in excellent agreement with the pseudogap determined from *transport* in LSCO and YBCO,[57] Fig. 8. In all three cases, the doping axis had to be scaled to cause the curves to coincide. The scaling suggests that, if the optimal doping for superconductivity in LSCO is $x=0.16$, it is an effective $x=0.2$ in YBCO, and $x=0.32$ in Bi-2212. Such a shift in x_c is consistent with the Uemura plot.[58] The scaling of x in Fig. 8 poses a complication for modelling the phase diagram: which x to choose for optimal doping. Here, we assume the correctness of the Uemura plot, and choose optimal doping

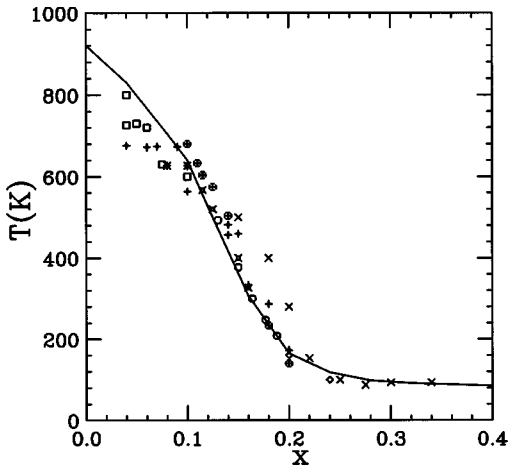

FIG. 8. Pseudogap phase diagram in LSCO and YBCO determined from transport. Open circles: from resistivity of YBCO; other symbols: transport measurements in LSCO, see Ref. 57; solid line from Fig. 7, with x axis scaled by a factor of 2.

to correspond to $x_{\rm opt}=0.32$; the problem is only in quantitative details, as an equally good fit can be made to $x_{\rm opt}\simeq 0.16$, Fig. 1 and Ref. 30. Figure 9 illustrates an optimized fit of the pBF model to the Bi-2212 pseudogap phase diagram. Details about choosing the parameters are discussed in Appendix A. Parameters are $t_0=0.25$ eV, $x_c=0.335$, $\omega_{\rm ph}=35$ meV, $\lambda_G=446$ meV, $\lambda_\Delta=194$ meV.

The overall qualitative and quantitative agreement is quite good. A number of features of the experimental data are worth commenting on. First, there is an approximately constant ratio between the total pseudogap, defined as the energy shift between the dispersion at $(\pi,0)$ and the Fermi level, and the pseudogap onset temperature T^*, $2\Delta(0)/k_BT^*\simeq 8$. A similar but smaller ratio, 4.1, is found in the calculation (note that this ratio is close to that found by Oda *et al.*[4]). Secondly, the overall shape of the curve, strongly x dependent in the underdoped regime, nearly constant in the overdoped regime, is well reproduced by the theory.

Finally, as noted previously,[8] there is excellent agreement between the photoemission pseudogap at $(\pi,0)$, $\Delta_{\rm PE}$, and the tunneling pseudogap, $\Delta_{\rm TU}$, defined as half the splitting between the two tunneling peaks. As illustrated in Fig. 5, this result is also in excellent agreement with theory. Note that the theory holds specifically *when the Fermi level is pinned at the VHC*. Indeed, we believe that the present data[8] constitute the strongest proof for this pinning. To illustrate the strength of the evidence, in the following subsection we will test the null hypothesis: assume that VH pinning is absent, and see how different $\Delta_{\rm PE}$ and $\Delta_{\rm TU}$ would be.

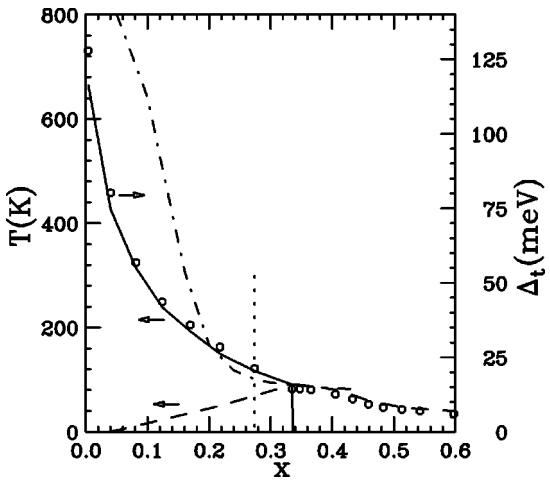

FIG. 9. Model pseudogap phase diagram for Bi-2212. Solid line =CDW transition T_p; dashed line=superconducting transition T_c; circles=total gap Δ_t at 1 K; dot-dashed line=solid line from Fig. 8.

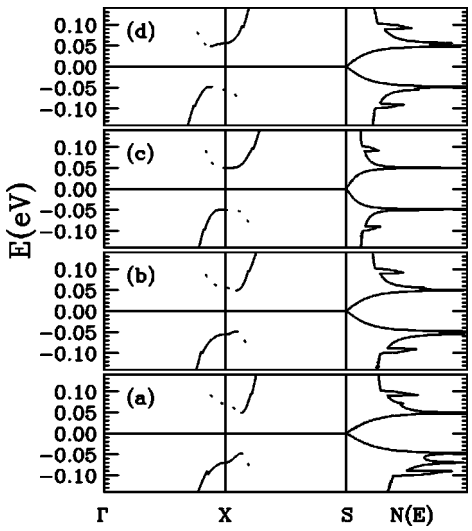

FIG. 10. Energy dispersion near the Fermi level (left), and associated tunneling density of states $N(E)$ (right) for a pure d-wave superconductor, as the VHS sweeps through the Fermi level: $(E_{\rm VHS}-E_F)/t=-0.2$ (a), -0.1 (b), 0 (c), $+0.1$ (d).

C. Van Hove pinning vs *d*-wave superconductivity

It has been suggested that what we have interpreted as Van Hove pinning can be alternatively explained as due to simple d-wave superconductivity, since the d-wave gap, $\Delta_d=\Delta_0(c_x-c_y)$ is largest near $(\pi,0)$. Here, we demonstrate that this is not the case. We assume that doping is accomplished by the filling of a rigid band, Eq. (2), and there is a fixed d-wave gap with doping-independent strength $2\Delta_0=50$ meV. Figure 10 illustrates the energy band dispersion near the Fermi level, and the corresponding tunneling spectra, at a series of dopings away from the VHS. The solid lines are the principal branches of the dispersion, with coherence factors $\geqslant 0.5$; the dashed lines are those parts of the ghost branches with coherence factors in the range 0.1–0.5. A large phonon energy $\hbar\omega_{\rm ph}=90$ meV was assumed, to shift the phonon peaks in the tunneling spectra out of the range of interest.

The tunneling spectra clearly show the VHS moving through the Fermi level. Note that the VHS is always at $(\pi,0)$, but the superconducting gap is at the Fermi level, and hence in general away from $(\pi,0)$. Superconductivity and the VHS actually produce two separate peaks in the tunneling spectra. (This fact has been noted earlier.[59]) If the spectra are too broadened to resolve the individual peaks, one would find the lower (upper) peak to be more intense in underdoped (overdoped) samples. This behavior is seen experimentally,[6,8] and constitutes strong evidence that at op-

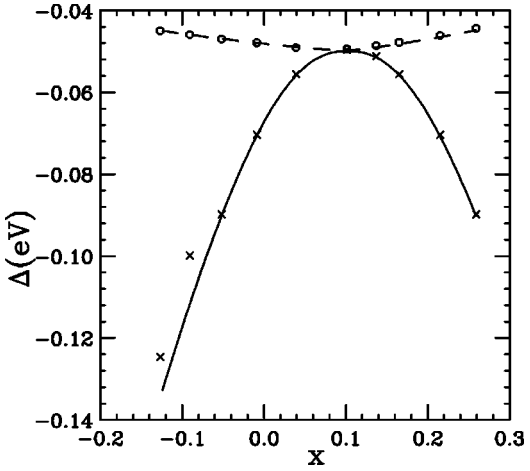

FIG. 11. Doping dependence of Δ_{TU} the tunneling (circles and dashed lines) and Δ_{PE}, the $(\pi,0)$ photoemission ($\times$ and solid curve) gaps, for a *d*-wave superconductor in the absence of VH pinning ($\tau=-0.25$).

timal doping the Fermi level exactly coincides with the VHS — in agreement with an earlier prediction.[60] We claim additionally that the Fermi level shifts away from the VHS anomalously slowly on the underdoped side.

It can be seen that the dominant gap arises away from the VHS — at the point where the bands cross the Fermi level. However, there is a subsidiary structure associated with the saddle point DOS peak, which rapidly shifts away from the Fermi level with doping. This would lead to a *double peak structure* in the tunneling spectrum. Moreover, it would mean that *the tunneling gap* (taken as the lower-energy, more prominent feature) *is distinct from the photoemission gap* [defined by the dispersion at $(\pi,0)$].

This is illustrated in Fig. 11, which shows the doping dependence of these two gaps. The symbols were estimated from the curves of Fig. 10 while the curves are analytical expressions, given by the curvature of the dispersion relations (Appendix B).

In Figure 12, we plot the calculated difference between

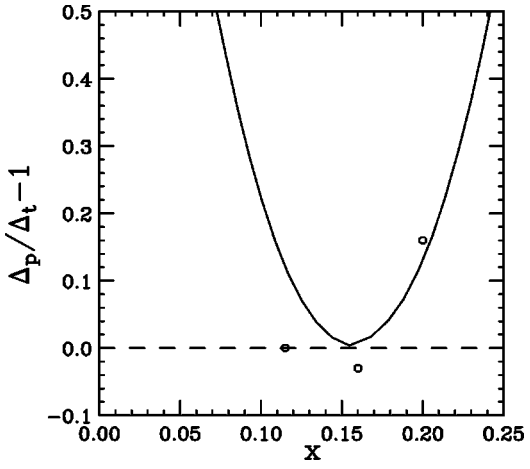

FIG. 12. Normalized splitting of Fermi level from the VHS, measured as the normalized difference between the tunneling and photoemission pseudogaps $(\Delta_{PE}-\Delta_{TU})/\Delta_{TU}$. Solid line=theory in the absence of pinning (similar to Fig. 11, but with $\tau=-0.38$); open circles=derived from data of Refs. 8 and 54.

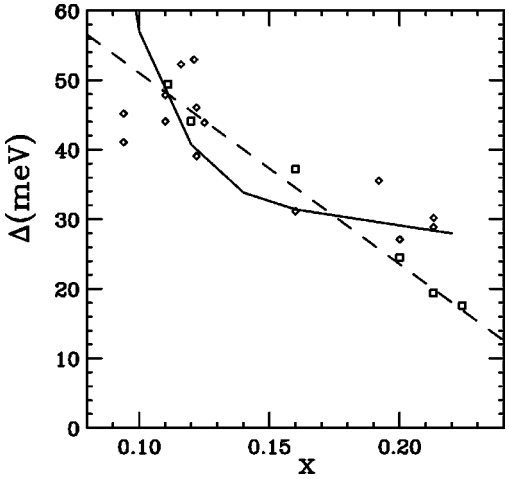

FIG. 13. Comparison of photoemission (diamonds) (Ref. 54) and tunneling (squares) (Ref. 8) gaps in Bi-2212. Solid and dashed lines=guides to the eye.

the tunneling and photoemission gaps, normalized to the tunneling gap, and compare this to our estimate of the *experimental* difference,[8] Fig. 7. For convenience, we replot the tunneling and photoemission gaps from Fig. 7 in Fig. 13. Only three data points could be extracted, and there are considerable error bars in the measurements. (Note in particular that $\Delta_{PE}-\Delta_{TU}$ cannot be negative.) The errors are smallest for the underdoped system: both tunneling and photoemission data are reported in Ref. 8, and are presumably for similar samples. In the other two systems, tunneling data from Ref. 8 are compared with photoemission data from Ref. 54.

Despite these limitations, the results are intriguing. There is a hint that the VHS depins from the Fermi level in the overdoped regime, but there is no sign of depinning in the underdoped samples. *Thus, the data appear to rule out the hypothesis of rigid band filling,* strongly implying that below optimal doping the Fermi level is pinned to the VHS. Clearly, this experiment needs to be repeated much more carefully, and over a wider doping range. In particular, (a) the photoemission gap must be measured exactly at $(\pi,0)$ and (b) both photoemission and tunneling must be carried out on the same (or identical) samples, to minimize sample-to-sample variations. However, a direct determination that the Fermi level is pinned to the VHS would confirm a number of strong correlation theories, and would have a profound influence on future theoretical modeling.

D. Tunneling spectra

Figure 14 illustrates the evolution of the calculated tunneling spectra with temperature in the underdoped regime ($x=0.274$, dotted line in Fig. 9). The dotted lines show the normal state VHS above T_p; the dashed lines are in the CDW phase; and the solid lines are in the mixed CDW-superconducting phase. The only broadening is thermal, due to the Fermi function; the disorder broadening $\Gamma=0$. As noted above [Fig. 5(b)], there are prominent features at the phonon frequency $\omega_{ph}=35$ meV (arrows). For a realistic phonon spectrum, they would split up into the strong-coupling factor α^2F. There have been a number of reports in the literature of the observation of such structure, but it is not clear how reproducible it is.

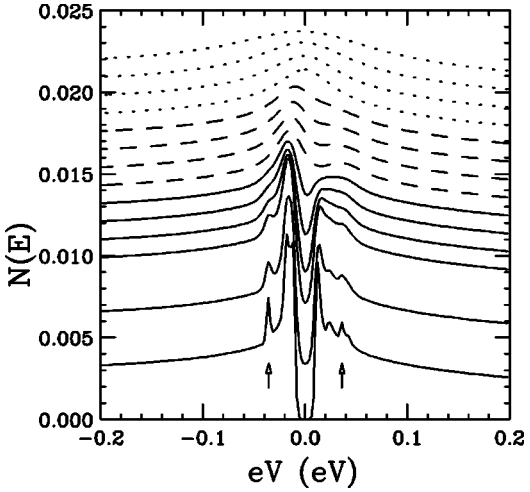

FIG. 14. Tunneling DOS for Bi-2212, using parameters of Fig. 9 (dotted line). From bottom to top, the temperatures vary from 10 to 100 K, in 10 K intervals, then go to 120, 150, 200, and 300 K. Dotted lines, $T>T_p=116$ K; dashed lines, $T_p>T>T_c=69$ K; solid lines, $T<T_c$. All curves are offset for clarity (all essentially coincide for $|eV|\geqslant 100$ meV).

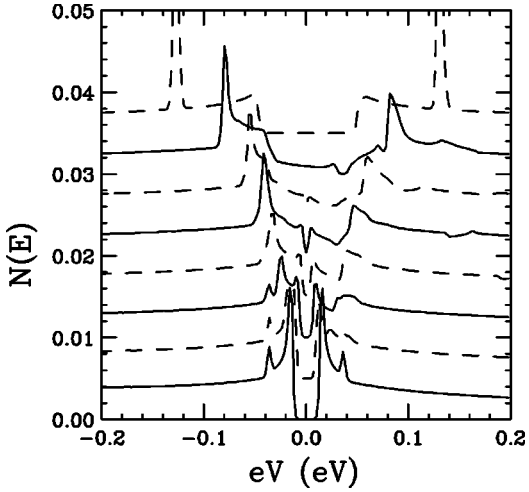

FIG. 16. Tunneling DOS for underdoped Bi-2212 at 10 K, as a function of doping, using parameters of Fig. 9. From top to bottom, the doping is $x=0.004$, 0.04, 0.08, 0.124, 0.169, 0.218, 0.274, and $x_c=0.34$. All curves are offset for clarity (all approximately coincide at eV=200 meV).

In order to better see the shape of the tunneling peaks, the DOS is recalculated in Fig. 15, with all parameters unchanged except $\hbar\omega_{\rm ph}=90$ meV. At 10 and 20 K, a splitting of the principal DOS peaks is just resolvable. The two peaks correspond to features *A* and *B* of Fig. 5 — that is, the larger peak is from the combined gap at $(\pi,0)$, the smaller from the superconducting gap near $(\pi/2,\pi/2)$. This splitting is essentially lost by 30 K, due to thermal broadening, and would not survive much disorder broadening. Note that the gap fills in with increasing temperature, without significantly closing. Indeed, since superconductivity disappears at a lower temperature, the gap actually appears to increase at higher temperatures. The low-temperature splitting increases with increased underdoping (Fig. 16), and hence might ultimately be observable experimentally. However, the data of Fig. 14 correspond to $T_c=69$ K, somewhat lower than any reported tunneling data. Moreover, the calculations are for an *s*-wave superconductor, and the smaller gap would be very different, or even absent, for a *d*-wave superconductor.

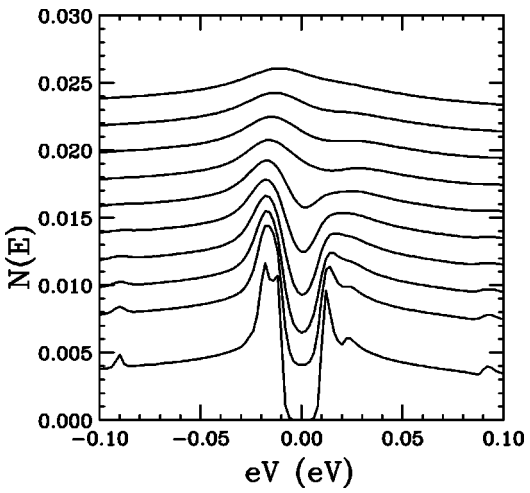

FIG. 15. Tunneling DOS for Bi-2212, using parameters of Fig. 14, but with $\hbar\omega_{\rm ph}=90$ meV. From bottom to top, the temperatures vary from 10 to 100 K, in 10 K intervals.

Thus, the model agrees with experiment[4] in finding gaplike features above T_c, but does not reproduce the rearrangement of features below T_c into a sharp peak, dip, plus hump. A suggested explanation for these features is given in the following section.

Figure 16 shows the evolution of the low-temperature tunneling spectra with doping, in the underdoped regime. At optimal doping (lowest curve) the gap is symmetrical and pure superconducting. As the material is successively underdoped, the peaks split, with the pseudogap peak growing and the superconducting peak shrinking, scaling with T_c, down to $x\simeq 0.06$ where superconductivity disappears.

The lowest doped state, close to half filling, is very interesting. For this state the present model is expected to be least accurate. The state is dominated by an electronic instability, the Mott transition. There is a charge-transfer gap of $\sim$1.6 eV, and a residual dispersion suggestive of the flux phase. Figure 17 shows that both these features are qualitatively present in the model. From Eq. (21), it can be seen that near half filling, when $t'\to 0$, the CDW gap opens up over the full Fermi surface, while the excess G_1 gap ensures that the largest gap is present near the VHS. The chief differences from experiment are (a) the gap evolves discontinuously from G_0 to G_0+G_1 rather than smoothly, (b) the overall bandwidth is too large, since the model has not taken into account that correlations renormalize the bandwidth from $\sim 8t$ to $\sim 2J$,[22] and (c) the model cannot reproduce the magnitude of the (electronic) Mott gap, $\sim$1.6 eV. Indeed, the full gap is limited to $\leqslant 2\hbar\omega_{\rm ph}$.

E. Peak, dip, and hump

The photoemission in Bi-2212 near $(\pi,0)$ has a characteristic shape in the superconducting state which is difficult to reproduce in the current model. In the pseudogap state above T_c, there is a very broad hump, consistent with a CDW gap with large broadening Γ, as in Sec. II D. In the

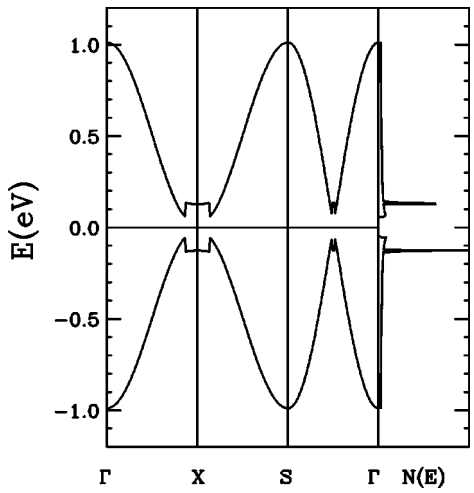

FIG. 17. Band dispersion near half filling Bi-2212 at 10 K, using parameters of Fig. 9.

superconducting state, the hump remains, but the low-energy side of the hump is transformed into a very sharp feature at energy Δ_1, with a dip at energy $\sim 2\Delta_1$. In the CDW superconductor, there is not expected to be such a two-peaked structure along $(\pi,0)$, but a single peak given by Eq. (1). However, as noted in Sec. II D, the broadening can have a strong energy dependence, with a long lifetime in the superconducting state cut off near 2Δ.[52] In the absence of a full theory, it is not clear which gap Δ represents, but since this is specifically a coherence effect, it seems reasonable to assume that it should be approximately the superconducting Δ_k. Since $\Delta_k < \Delta_t$, one can get a behavior at low temperatures which is closer to experiment. Figure 18 illustrates the three possible behaviors, depending on whether $2\Delta_k$ is $\ll$, $\sim <$, or $> \Delta_t$: one can get hump plus dip (dotted line), hump plus peak (dashed line), or peak plus dip (solid line). In the last case, the dip is not necessarily at twice the peak in energy.

It seems clear, however, that the hump is associated with the pseudogap, and the peak with the superconducting gap.

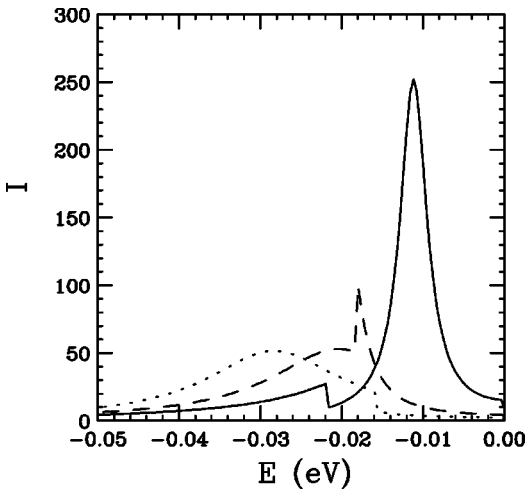

FIG. 18. $(\pi,0)$ photoemission spectra for Bi-2212 at $T=1$ K, using parameters of Fig. 9 ($x=0.22$), except $\lambda_G=0.446$ (dotted line), 0.385 (dashed line), and 0.325 eV (solid line). Broadening given by Eq. (23).

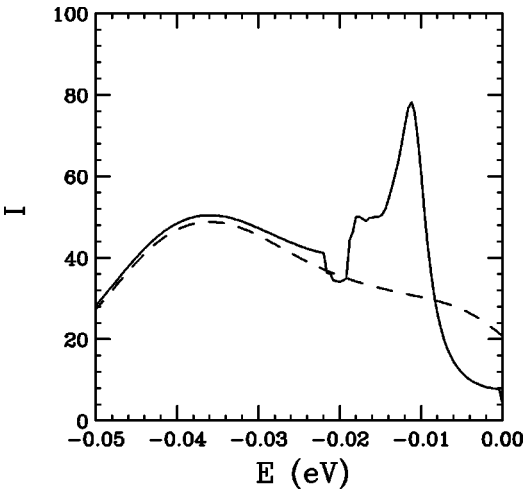

FIG. 19. $(\pi,0)$ photoemission spectra for Bi-2212, using parameters of Fig. 9 ($x=0.22$), except inhomogeneously broadened (averaged over $20\lambda_G$ values, chosen to give pseudogap onset temperatures uniformly spaced between 60 and 250 K). Solid line: $T=1$ K, dashed line: $T=70$ K.

We suggest that the experimental result may represent an effect of phase separation, which is not well captured by our model. To test this hypothesis, we developed a simple model, assuming that the pseudogap feature is inhomogeneously broadened. Specifically, we assume that T_p is spatially inhomogeneous, and that regions of different T_p evolve independently. Physically, this spread could be associated with regions of varying hole density, as in stripes. For simplicity, we model the spread in T_p by varying λ_G.

For each separate microregion, lowering the temperature will produce a spectrum such as one of those in Fig. 18. In the regions of large λ_G, superconductivity has little effect, leaving the hump unchanged. However, when λ_G is small, at low T there will be a sharp superconducting peak plus well-defined dip. Figure 19 shows the resulting spectra, both just above the onset of superconductivity, at $T=70$ K (dashed line), and at low temperature, $T=1$ K (solid line). Each spectrum is the superposition of 20 individual spectra, with T_p varying in 10° steps about the average value, 150 K. For all spectra, the broadening is taken as

$$\Gamma = \begin{cases} \Gamma_1 & \text{if } |E| \leqslant 2\Delta_k, \\ \Gamma_2 & \text{otherwise,} \end{cases} \tag{23}$$

with $\Gamma_1=2$ meV, $\Gamma_2=10$ meV. The general features of the experiment are clearly reproduced, although the sharp peak is not resolution limited, due to the inhomogeneous broadening.

This interpretation of the sharp peak as a measure of Δ_k leads to a new problem, since the experiments imply that this Δ_k increases with decreasing x. To reproduce this behavior in the phase diagram would require that λ_Δ varies with doping — the same effect needed to explain the LSCO phase diagram, Fig. 3. Such a doping dependence would be consistent with magnetic fluctuation-induced superconductivity. However, it must be kept in mind that an alternative interpretation, such as the solid line in Fig. 18, was ruled out because the dip feature falls at exactly $2\Delta_1$. There exist some data (e.g., Fig. 1 of Ref. 46) in which the dip falls at an

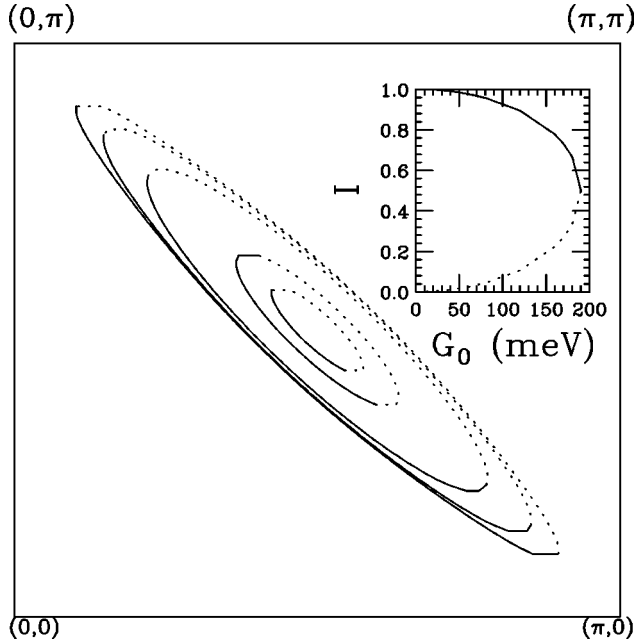

FIG. 20. Fermi surface in CDW phase, for $\tau=-0.38$, $G_0=20$, 40, 80, 160, and 180 meV, for progressively smaller ellipses. Dotted segments=ghost Fermi surfaces, with coherence factors <0.5. Inset: coherence factors along the diagonal ($k_x=k_y$).

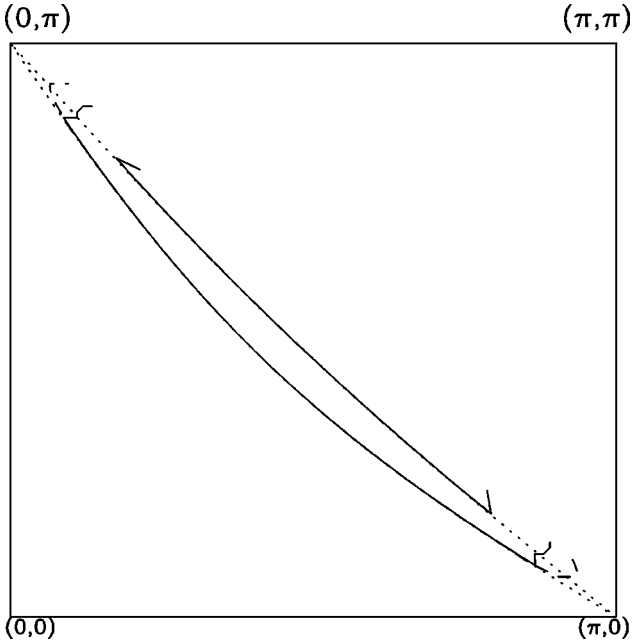

FIG. 21. Fermi surfaces in CDW phase, for self-consistent parameters. Lower (upper) set of lines: $\tau=-0.4$ (-0.16), $\lambda_G=0.50$ (0.25) eV. Dotted lines=in normal state above T_p; solid lines=in pseudogap state, just above T_c; dashed lines=intermediate temperatures. Only segments of Fermi surface with coherence factors $\geqslant 0.1$ are shown.

energy substantially less than $2\Delta_1$. This discrepancy must be clarified before a definitive model for the sharp peak can be established.

F. The incredible shrinking Fermi surface

Norman *et al.*[61] have shown that the Fermi surface in the pseudogap phase has a remarkable temperature dependence: there is a full, large Fermi surface above the pseudogap transition, T_p, but as T is reduced below T_p, the Fermi surface gradually collapses — vanishing first near $(\pi,0)$ and then over a larger angular range before ultimately being reduced to a point along the line $c_x=c_y$. This low-temperature limit is consistent with a *d*-wave superconductor, but the intermediate-temperature regime is not: the gap should open at T_c everywhere on the Fermi surface, with the magnitude of the gap proportional to (c_x-c_y). Fluctuation broadening could produce this effect by limiting the pseudogap to those parts of the Fermi surface where it is larger than the energy uncertainty.[62–64] However, it can also be interpreted in terms of a VH nesting gap.

Figure 20 shows the evolution of the Fermi surface with G_0, for $\Delta=G_1=0$. In a pure CDW state, the Fermi surface can be calculated analytically, Appendix C. For finite G_0, the surface is an ellipse, with the inner half derived from the original Fermi surface and the outer half a ghost Fermi surface, zone folded by Q. The latter has considerably lower intensity (inset), and will be further reduced by fluctuation effects and stripe effects; it is not seen experimentally. On the other hand, the truncated original surface has a large coherence factor ($\geqslant 0.5$), and bears a strong resemblance to the experimental data. Below T_c, the G_i's shrink as Δ grows, so the opening of the superconducting gap takes over. Thus, for a *d*-wave superconductor, the residual points of zero gap would lie along the original Fermi surface, as observed, and not at $(\pi/2,\pi/2)$. When $G_1\neq 0$, Fig. 21, the resemblance to experiment is even closer: the Fermi surface shrinks down with essentially no change of shape, from the pseudogap onset to the superconducting T_c.

There is one possibly significant difference: as the normal state above T_p is approached, Fermi surfaces should approach the VHS's at $(\pi,0)$, which is not clearly seen in experiment. A related problem is the minimum gap locus found in the pseudogap phase. These problems will be discussed further in the following section.

G. Minimum gap locus

In order to recover a ''Fermi surface'' in the presence of a (pseudo) gap, Ding *et al.*[65] have introduced the concept of a ''locus of minimum gap.'' For a series of cuts in the Brillouin zone, they define the minimum gap — the $\vec{k}$ point at which the photoemission gap most closely approaches the Fermi level. The gap is defined as the leading edge of the photoemission pattern, but the comparison with tunneling[8] suggests that the peak position should work as well. The Fermi surface would then correspond to a locus of zero-gap excitations. In Appendix C, analytical expressions for the Fermi surface and minimum gap locus (actually, the maximum in the dispersion of the lower band) are derived, which are plotted as lines in Fig. 22. The solid lines are the Fermi surface, the dashed lines the minimum gap loci, and the dot-dashed and dotted lines their ghostly counterparts. Neglecting the ghost surfaces, the resulting dispersion resembles the experimental findings.[65] Note in particular that the locus of minimum gap does *not* pass through the $(\pi,0)$ point, even though ϵ_F is pinned at the VHC [see Eq. (C4)]. This can readily be understood: since the gap is largest at $(\pi,0)$, the

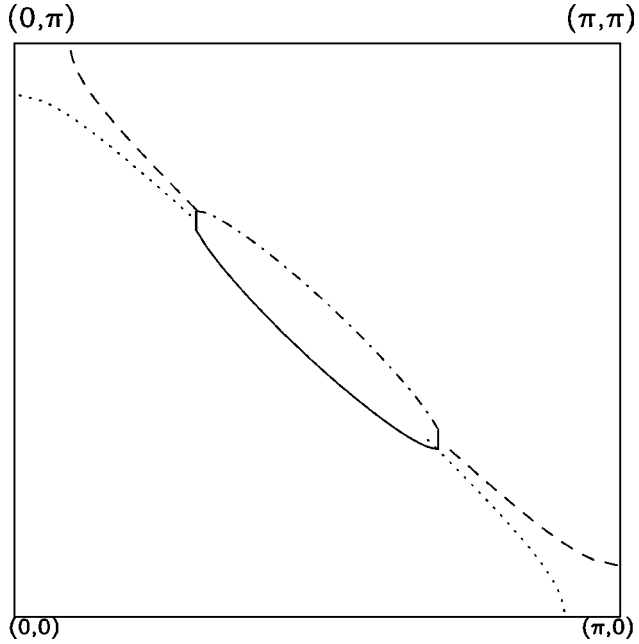

FIG. 22. Loci of minimum gap (dashed and dotted lines) and zero gap (solid and dot-dashed lines). Parameters are $\tau=-0.45$, $G_0=40$ meV, $G_1=\Delta_k=0$.

scans find a smaller gap at some k_x away from this point. Knowing the full dispersion $E(\vec{k})$, a much fuller test of the theory can in principle be carried out.

While the problem of the minimum gap locus can be satisfactorily explained in the pinned VHS model, the problem remains that in the normal state above the pseudogap, the Fermi surface found in photoemission does not seem to intersect $(\pi,0)$. It must be recalled that the VHS is the ultimate hot spot, so local residual disorder is likely to broaden or split the quasiparticle spectrum near the VHS even at temperatures considerably in excess of the pseudogap temperature. An indication for such smearing is the disagreement between the Argonne[65] and Stanford[1] groups on the shape of the Fermi surface near the VHS in underdoped cuprates. Hence we prefer to infer the position of the VHC from data in the superconducting state, when line broadening effects are smallest. If the VHC is within 5 meV of ϵ_F in the superconducting state (Fig. 12), it should be even closer in the normal state, since the superconducting transition tends to shift the chemical potential away from the VHS.[66]

H. Spectral weight shift

Shen *et al.*[67] have recently found significant shifts of spectral weight on cooling the sample from the pseudogap phase above T_c to the superconducting phase below. These are exactly the sort of changes one would expect in the present model, since the CDW and superconductivity have very different gap structures, and the CDW gap is significantly *reduced* below T_c, Fig. 2. However, experimentally these changes are found to occur over an energy range extending to ~ 300 meV away from ϵ_F. This extended range is presumably telling us about the relevant pairing bosons, but since these energies are greater than $\hbar\omega_{\rm ph}$, strong coupling calculations are required, which are beyond the scope of the present paper.

IV. CONCLUSIONS

We have taken a simple pinned Van Hove ansatz for the striped pseudogap phase in the cuprates, and analyzed the predicted tunneling and photoemission spectra, comparing them with experimental data. Highlights of our results include the following. (1) We explain the experimental observation that the tunneling peaks coincide with the $(\pi,0)$ photoemission dispersion, and show that careful measurements of this effect can provide direct evidence of pinning of the Fermi level to the VHC over an extended doping range. (2) In turn, the fact that tunneling shows a well-defined gaplike feature confirms that the $(\pi,0)$ dispersion also has two branches — that is, that the pseudogap is associated with some form of VHS nesting.[22] (3) The tunneling gap has a characteristic asymmetry which vanishes at optimal doping; this is evidence that optimal doping is that point at which the Fermi level exactly coincides with the VHS.[60]

(4) By plotting the doping dependence of the photoemission hump feature, the resulting pseudogap phase diagram for Bi-2212 is in good agreement with similar phase diagrams for LSCO and YBCO, derived from transport measurements. Since the scaled data in Fig. 8 all have optimal doping values x_c consistent with the Uemura plot, the possibility arises that *the pseudogap phase diagram may be universal, while optimal doping x_c varies from compound to compound*. (5) The rearrangement of spectral weight seen below T_c can be interpreted as a generation of separate pseudogap (hump feature) and superconducting (sharp feature) peaks with the dip between them due to superconducting coherence effects. However, this requires inhomogeneity not included in the simple Ansatz. (6) Finally, a number of specific features observed in the photoemission receive a natural explanation in this model, including the shrinking Fermi surface and the locus of minimum gap.

A shortcoming of the model is the prediction of a splitting of the tunneling gap, which has not yet been observed. However, we note that (a) this may be due to the assumption of *s*-wave superconductivity, and (b) even the assumption of a pure *d*-wave superconductor, with no pseudogap, would lead to a split peak in tunneling unless the Fermi level were pinned to the VHS.

V. DISCUSSION

A. Alternative pseudogap scenarios

The present interpretation of the pseudogap in terms of Van Hove nesting is in agreement with some early (1990) calculations[68,39] which predated any of the experimental observations of the ''spin gap'' or pseudogap. However, one of these theories involves an SDW,[68] the other a CDW,[39] while more recent calculations[20–22] involve a flux phase near half filling. Hence, the essential feature is the Van Hove nesting; the particular instability depends on the details of the electron-electron interaction.

It is convenient to classify these instabilities in terms of the SO(6) scenario. As discussed in Sec. II B, the instabilities fall into two broad classes: nesting and pairing. We expect that the phase diagram, Fig. 1, of the competition between pseudogap and superconductivity, would not be greatly changed if the pseudogap represents any *nesting* instability,

as long as the physics is dominated by proximity to a VHS. This would hold for any Hubbard or tJ model, in which the VHS is at half filling, and more particularly for any model which introduces a higher order hopping parameter (t' or t_{OO}) to move the VHS toward finite positive x (hole doping) —i.e., closer to optimal doping.

Among the *nesting* theories of the pseudogap, we include Schrieffer's spin bag[68] and Zhang's SO(5),[13] for which the instability is an SDW, Laughlin's[20] and Wen and Lee's[21] flux phase models, and Klemm's CDW model.[69] Within an SO(6) symmetric model, all would produce the same pseudogap phase diagram. Hence, the question of which one actually produces the ground state depends on which symmetry-breaking operators are present in the physical cuprates.

Following the discussion in Sec. II B, it would be more difficult to reproduce the pseuodgap phase diagram in terms of a *pairing instability* — i.e., assuming that the pseudogap is a signature of superconducting fluctuations, a precursor of real space pairing. We believe that this class of models will have difficulty explaining striped phases, and the seemingly smooth extrapolation of the pseudogap to the SCOC dispersion at half filling. On the other hand, some recent models[70,71] have incorporated a preformed pair or fluctuating regime as part of a crossover from superconductivity at optimal doping to a Néel or staggered flux phase near half filling. These models are much closer to the spirit of the present calculation, but have not so far calculated how this crossover affects the tunneling and photoemission spectra.

B. Distinguishing the nesting instabilities

There is a natural generalization[72] of Eq. (1) to SO(6),

$$\Delta_t = \sqrt{\sum_{i=1}^{12} \Delta_i^2}, \tag{24}$$

where the sum is over all twelve instabilities of both superspins. Thus, *at* $(\pi,0)$ *the pseudogap depends only on the vector sum of the individual gaps*. For $t'=0$, Eq. (24) holds over the full Fermi surface. Hence, the instabilities can only be distinguished by their dispersion away from $(\pi,0)$.

In attempting to distinguish different models, it must be kept in mind that this secondary dispersion is likely to be model dependent. For example, *d*-wave superconductivity would have different dispersion depending whether it was phonon-induced or an electronic instability. The dispersion will be sensitive to the nature of the boson mediating superconductivity, in particular to the cutoff ω_c.

A second example is instructive. In the antiferromagnetic state at half filling there is a competition between the Néel phase (commensurate SDW) and the flux phase. In a Hartree-Fock calculation, both phases give rise to similar gaps at $(\pi,0)$, but have very different dispersion in other directions. In particular, the Néel gap is approximately isotropic, while the flux phase has zero gap near $(\pi/2,\pi/2)$, and closely resembles the experimental dispersion of SCOC.[19] (See Fig. 32 of Ref. 18 and the associated discussion for references to earlier literature.) This is suprising, since the Néel phase should be more stable, having the larger average gap, and it was speculated that the Néel phase dispersion is modified by fluctuation or correlation effects. This seems to be the case, since calculations of the dispersion of one hole in an antiferromagnet are capable of reproducing the experimental dispersion.[73] Thus, while the theoretical interpretation has proven quite involved, the dispersion remains simple: it has the periodicity of the Néel superlattice, with maximal gap associated with VHS splitting.

Despite these caveats, we are exploring an SO(6)-generalized version of the pBF model, to test how sensitive the phase diagram and tunneling and photoemission spectra are to the particular forms of nesting or pairing instabilities.

C. Is there a phase transition at the pseudogap?

It must be kept in mind that the present calculations are mean-field, and thus find a true gap opening at T_p, rather than a pseudogap. Inclusion of fluctuations would bring about the following changes.[68,39] (1) In two dimensions, the Mermin-Wagner theorem shows that fluctuations destroy long-range CDW or SDW order. (2) Thus, in a purely two-dimensional system, a pseudogap would open close to the mean-field T_p, but a true gap would emerge only at $T=0$. (3) Three-dimensional correlations could bring about true long-range order at some $T_{3D} \ll T_p$. (4) The cuprate pseudogap provides one additional complication: stripes. In a classical picture of phase separation, the pseudogap onset would be accompanied by a spinodal decomposition into magnetic and hole-doped (CDW)[22] domains, with attendant large increase of fluctuation disorder. The quantum version of spinodal decomposition, with strong Coulomb effects, is yet to be worked out.

In light of the above, long-range pseudogap order is not necessarily expected, but can arise in special circumstances. Is there any sign of this in the cuprates? There are several features which may be suggestive of such effects, albeit usually in special limits. (a) In $La_2CuO_{4+\delta}$, the interstitial oxygens are mobile below room temperature, and a macroscopic spinodal decomposition takes place below ~ 415 K.[74] Interestingly, the phase separation seems to coincide with a structural phase transition. (b) In $YBa_2Cu_4O_8$, the double chains show negligible oxygen vacancy disorder, but the stoichiometric compound is intrinsically underdoped, with pseudogap comparable to $YBCO_{6.6}$. There are reports that Ca substituted samples show a structural phase transition with long-range order near the pseudogap temperature.[75] (c) The low-temperature orthorhombic (LTO) transition in LSCO has a very similar doping dependence to the pseudogap, but with $T_{\rm LTO} \sim T_p/2$ [Fig. 52a of Ref. 18]. The pseudogap, LTO, and related low-temperature tetragonal (LTT) phases have been interpreted as a series of dynamical and static Jahn-Teller phases,[43] which in the present context would correspond to increasingly ordered versions of the CDW phases. (d) Finally, the LTT phase can be stabilized to give a long-range ordered phase near the 1/8 anomaly in LSCO:Nd and in $La_{2-x}Ba_xCuO_4$. At the same time there is long-ranged stripe order and long-ranged antiferromagnetic order. It is tempting to assume that the antiferromagnetic order is associated with the undoped stripes, and the LTT order with the hole-doped stripes, in accord with prediction.[24,22] Additional information on the connection between the pseudogap and structural ordering is discussed in Sec. 9.1 of Ref. 18.

D. Doping dependence of λ_Δ

There were a few tantalizing hints that the superconducting coupling parameter λ_Δ is doping dependent: increasing as x is reduced below optimal doping. This was needed to explain the LSCO phase diagram, Fig. 3, and the doping dependence of the sharp photoemission peak below T_c, Sec. III E. This could have a simple explanation — e.g., the bandwidth is reduced by correlation effects from $\sim 4t$ (half bandwidth) at optimal doping to $\sim 2J$ near half filling, and this reduction is neglected in the pBF model. Alternatively, it could signal the importance of magnetic fluctuations.

In the three-band slave boson model calculation,[22] the stripes were interpreted as a crossover from a flux phase near half filling to a CDW phase near optimal doping. In SO(6), this is a crossover between the two different superspin multiplets, and is accompanied by a crossover from *d*-wave to *s*-wave superconductivity. This would be consistent with hints of a more *s*-wave-like superconducting transition in overdoped materials.

Recently, a number of relevant results have appeared.

(1) Panagopoulos and Xiang[76] have determined that the slope of the gap near the gap zero at $(\pi/2,\pi/2)$ scales with T_c, and not with the gap near $(\pi,0)$. Similarly, Mourachkine[77] has found evidence for two tunneling gaps, very similar to features *A* and *B* of Fig. 5; as predicted, feature *B* scales with T_c, and not with the pseudogap, feature *A*.

(2) Miyakawa *et al.*[78] provide additional data on the tunneling gap, suggestive of significant superconducting fluctuations. However, a careful analysis[79] finds deviations from scaling of the dip feature with the tunneling gap, which can be interpreted as due to a significant non-superconducting component of the gap, which grows significantly with underdoping.

(3) Corson *et al.*[80] find direct evidence for superconducting fluctuations and a Berezinski-Kosterlitz-Thouless transition, from which they can estimate a bare superconducting transition temperature $T_{c0} > T_c$. However, T_{c0} is considerably smaller than the pseudogap onset — in fact, T_{c0} decreases with increased underdoping, like T_c, but unlike the pseudogap. Their data are for samples with $33\ \mathrm{K} \leqslant T_c \leqslant 71$ K, and hence are not inconsistent with Miyakawa *et al.*,[78] who study $T_c \geqslant 70$ K. Indeed, the analysis of Ref. 79 suggests a maximum in T_{c0} near 70 K.

(4) Parker *et al.*[81] have used a novel approach to attaching contacts, which appears to enhance the pseudogap contribution to tunneling. The temperature dependence of their tunneling spectra resembles Fig. 19, with only a weak dip feature but with a pronounced pseudogap contribution above T_c.

ACKNOWLEDGMENTS

We would like to thank NATO for enabling A.M. Gabovich to visit us and discuss his work.

APPENDIX A: PHASE DIAGRAM FOR LSCO AND YBCO

We briefly discuss the procedure for determining the phase diagram of Figs. 1–3 and 9, to indicate the role of the various parameters.

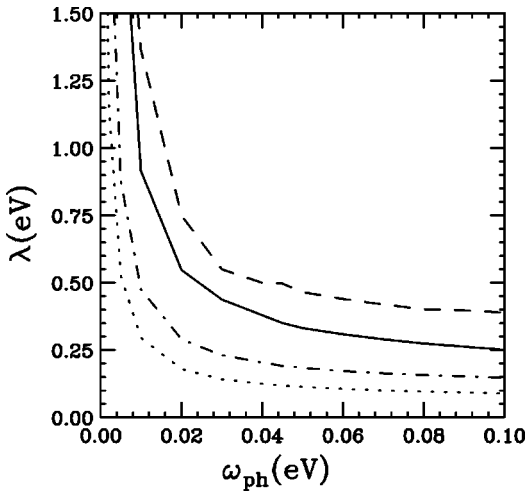

FIG. 23. Allowed values of λ vs $\omega_{\rm ph}$ to fix $T_p = T_c = 90$ K at optimal doping. Solid (dashed) line $= \lambda_G$ for $\tau = -0.6$ (-0.9); dot-dashed (dotted) line $= \lambda\Delta$ for $\tau = -0.6$ (-0.9).

1. Choice of τ

Using Eq. (3), a value $\tau = 2t'/t = -0.38$ is necessary for the VHS to fall at optimal doping $x_c = 0.16$ in LSCO. On the other hand, there is a suggestion[82] that τ in LSCO may be as large as -0.6, which corresponds to $x_c = 0.274$.

In YBCO, band structure calculations suggest $\tau = -0.9$ — remarkably close to the critical value -1.0 for one-dimensional behavior. This in turn corresponds to a doping $x_c = 0.54$. Note, however, that the band structure calculations also find a significant interplane coupling between the two CuO_2 planes in a unit cell, such that the symmetrical combination is essentially undoped. In this case, for the antisymmetrical combination Fermi surface to be at the VHS would require an average doping per layer of $0.54/2 = 0.27$ holes. This is consistent with the optimal doping estimated from the Uemura plot,[58] which finds that x_c/m is about twice as large for YBCO as for LSCO. Assuming that both materials have the same effective mass m, this would give a broad peak in x_c near 0.32 for YBCO.

The situation for Bi-2212 is slightly more complicated. The Uemura plot suggests an x_c similar to that in YBCO, while photoemission is consistent with $\tau \simeq -0.9$.[65] However, there is no evidence in photoemission for the interlayer splitting of the Fermi surface. We will postulate that a splitting similar to that found in YBCO is locally present, but is obscured by a very short *c*-axis correlation length.

2. Optimal doping

In YBCO, the pseudogap appears to vanish very close to optimal doping, as soon as the superconducting T_c exceeds the pseudogap T_p. This is a natural consequence of the BF model, and so is a convenient point to fix for the phase diagram. We proceed as follows. For a given τ, we set the Fermi level at the VHS and calculate the electron-phonon coupling energies λ_Δ and λ_G which give $\Delta_k = G_k = 0^+$ at $T = 90$ K. With this choice of λ's, $T_c = T_p = 90$ K at this doping, and at any larger doping the pseudogap will be suppressed to zero by T_c. The only free parameter is $\omega_{\rm ph}$. In Fig. 23, we plot the resulting λ's vs $\omega_{\rm ph}$ for two choices of τ.

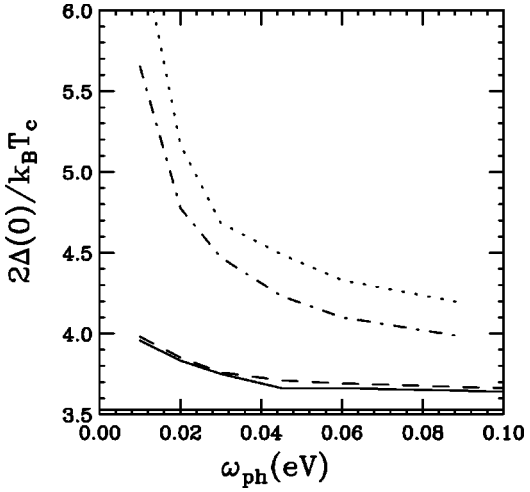

FIG. 24. Gap ratio vs $\omega_{\rm ph}$ using values of λ determined from Fig. 23. Solid (dashed) line=ratios for superconducting gap for $\tau=-0.6$ (-0.9); dot-dashed (dotted) line=ratios for CDW gap for $\tau=-0.6$ (-0.9).

As expected, for a larger $\omega_{\rm ph}$, a smaller λ is needed, but for $\omega_{\rm ph}>30$ meV, the value of λ varies only weakly. The dependence of the λ's on τ is what would be expected from Fig. 1: nesting is strongest for $\tau=0$, so the necessary λ_G increases with increasing τ, while pairing becomes easier as the bands become more one-dimensional, $\tau\rightarrow 1$.

3. Choosing $\omega_{\rm ph}$

If we assume $t=0.25$ eV is known, and that λ_Δ and λ_G are doping independent, there is only one remaining free parameter $\omega_{\rm ph}$ to adjust to fit the rest of the phase diagram. We explore three features in particular: the gap ratio, the magnitude of the limiting pseudogap at zero doping, and the superconducting onset.

In weak coupling BCS theory, the gap ratio $2\Delta(T=0)/k_BT_c=3.53$, and increases for stronger coupling. Figure 24 shows the variation of this ratio with $\omega_{\rm ph}$, where the λ's are fixed by Fig. 23, as discussed above. The ratio for the superconducting phase is somewhat enhanced from the BCS value, and depends only weakly on $\omega_{\rm ph}$. The ratio can be much larger and more $\omega_{\rm ph}$-dependent for the pseudogap. Note that in Fig. 1, where $\lambda_\Delta=\lambda_G$ is assumed, the two gap ratios are nearly equal. (The problem with Fig. 1 is that the critical doping is too low.) Experimentally, Oda *et al.*[4] find a value 4–5, whereas the data of Ding *et al.*[54] yield ~ 8. Thus, the model can account for the former value, but not the latter. If the correct ratio turns out to be ~ 8, this may be evidence for pair-breaking effects limiting T_c.[83]

Figure 25 shows how the limiting pseudogap $T_p(\tau=0)$ depends on $\omega_{\rm ph}$ (in view of the uncertainty in the gap ratio, we have chosen to work with the critical temperature rather than the gap). Another constraint is the superconducting onset $x_{\rm min}$, the doping at which superconductivity first appears. This is ~ 0.05 in LSCO; for YBCO and Bi-2212, it is hard to specify the precise planar hole doping. Adjusting $x_{\rm min}$ is somewhat in conflict with the other constraints, since a large difference $\lambda_G-\lambda_\Delta$ leads to a larger $x_{\rm min}$, Fig. 26. Given these conflicting constraints, the parameters of Fig. 9 seem to provide the best overall solution.

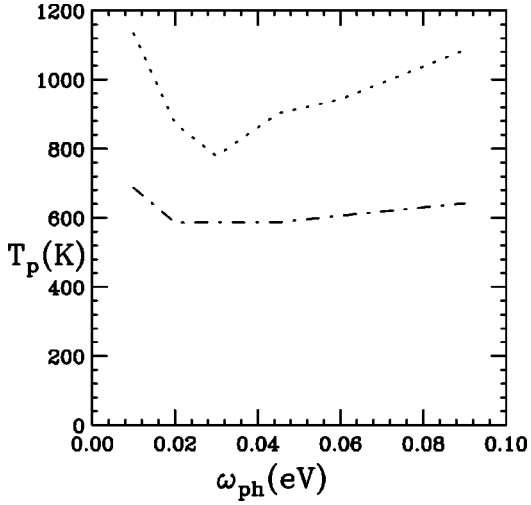

FIG. 25. CDW onset T_p at zero doping vs $\omega_{\rm ph}$ using values of λ determined from Fig. 23. Dotdashed (dotted) line=T_p for CDW gap for $\tau=-0.6$ (-0.9).

APPENDIX B: ANALYSIS OF *d*-WAVE GAPS

For a purely superconducting gap ($G_0=G_1=0$) the eigenvalues of Eq. (6) simplify:

$$E_\pm=\pm\sqrt{(\epsilon_k-\epsilon_F)^2+\Delta_{\vec{k}}^2}. \tag{B1}$$

For a *d*-wave superconductor, $\Delta_{\vec{k}}=\Theta_{\vec{k}}\Delta_0(c_x-c_y)$. The tunneling peak corresponds to the maximum of E_- (or minimum of E_+). From Fig. 10, it is sufficient to evaluate $\partial E_-/\partial c_x$ when $c_y=\pm 1$ (the $+1$ solution corresponds to overdoping, -1 to underdoping). In terms of the scaled variables $\tau=2t'/t$, $\delta=\Delta_0/2t$, and $\hat{\mu}=\epsilon_F/2t$, the maximum occurs at

$$\pm c_x=\frac{\delta^2-(1\pm\tau)(1\pm\hat{\mu})}{\delta^2+(1\pm\tau)^2}, \tag{B2}$$

and is $E_{\rm max}\equiv\Delta_{\rm TU}$ with

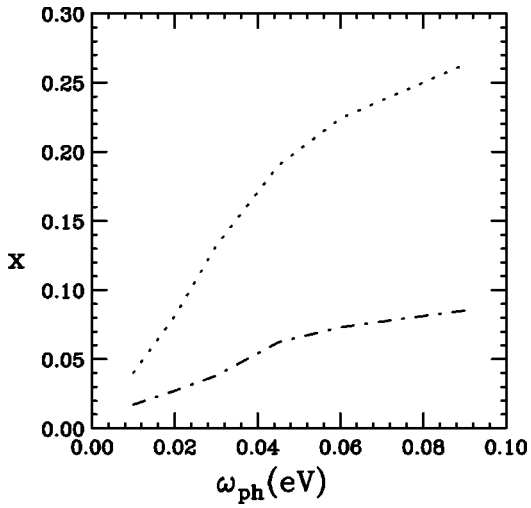

FIG. 26. Onset of superconductivity x vs $\omega_{\rm ph}$ using values of λ determined from Fig. 23. Dot-dashed (dotted) line=x for CDW gap for $\tau=-0.6$ (-0.9).

$$\left(\frac{E_{\max}}{2t}\right)^2=\frac{\delta^2(\tau+\hat{\mu}\pm 2)^2}{\delta^2+(1\pm\tau)^2}, \tag{B3}$$

which give the dashed lines in Fig. 11. The photoemission gap $\Delta_{\rm PE}$ (solid line in Fig. 11) is simply the value of E_- at $(\pi,0)$:

$$\left(\frac{\Delta_{\rm PE}}{2t}\right)^2=(\tau-\hat{\mu})^2+4\delta^2. \tag{B4}$$

When the Fermi level coincides with the VHS, $\hat{\mu}=\tau$, and $\Delta_{\rm PE}=\Delta_{\rm TU}=2\Delta_0$, to lowest order in δ^2.

APPENDIX C: PROPERTIES OF THE CDW

When superconductivity is absent, the Fermi surface can be found from solutions to

$$\tilde{\epsilon}_{\vec{k}}\tilde{\epsilon}_{\vec{k}+\vec{Q}}=G_{\vec{k}}^2, \tag{C1}$$

where $\tilde{\epsilon}_{\vec{k}}=\epsilon_{\vec{k}}-\epsilon_F$. When the Fermi level is pinned at the VHS, $\epsilon_F=4t'$, this reduces to

$$c_x=\frac{-(1-\tau^2)c_y\pm\sqrt{\tau^2 s_y^4-g^2(1-\tau^2c_y^2)}}{1-\tau^2c_y^2}, \tag{C2}$$

using $s_y^2=1-c_y^2$ and $g=G_{\vec{k}}/2t$, in addition to the notation introduced in Appendix B. The Fermi surface shrinks to the point $(\pi/2,\pi/2)$ when $g=|\tau|$.

The locus of minimal gap can be found as in Appendix B. Its exact position depends on the orientation of the scan. Here, we fix k_y and scan k_x. The top of the E_{k-} band is then at

$$c_x=-c_y\pm\frac{|\tau g c_y|}{\sqrt{1-\tau^2c_y^2}}. \tag{C3}$$

In particular, for $c_y=1$

$$c_x=-1+\frac{|\tau g|}{\sqrt{1-\tau^2}}. \tag{C4}$$

Note that, even though the Fermi level is pinned at the VHC, the locus of minimum gap does not pass through $(\pi,0)$.

*On leave of absence from Inst. of Atomic Physics, Bucharest, Romania.

[1] D.S. Marshall, D.S. Dessau, A.G. Loeser, C.-H. Park, A.Y. Matsuura, J.N. Eckstein, I. Bozovic, P. Fournier, A. Kapitulnik, W.E. Spicer, and Z.-X. Shen, Phys. Rev. Lett. **76**, 4841 (1996).

[2] A.G. Loeser, Z.-X. Shen, and D.S. Dessau, Physica C **263**, 208 (1996); A.G. Loeser, Z.-X. Shen, D.S. Dessau, D.S. Marshall, C.H. Park, P. Fournier, and A. Kapitulnik, Science **273**, 325 (1996).

[3] H. Ding, T. Yokoya, J.C. Campuzano, T. Takahashi, M. Randeria, M.R. Norman, T. Mochiku, K. Kadowaki, and J. Giapintzakis, Nature (London) **382**, 51 (1996).

[4] M. Oda, K. Hoya, R. Kubota, C. Manabe, N. Momono, T. Nakano, and M. Ido, Physica C **281**, 135 (1997).

[5] H.J. Tao, F. Lu, and E.L. Wolf, Physica C **282-287**, 282 (1997).

[6] Ch. Renner, B. Revaz, J.-Y. Genoud, K. Kadowaki, and O. Fischer, Phys. Rev. Lett. **80**, 149 (1998).

[7] Y. DeWilde, N. Miyakawa, P. Guptasarma, M. Iavarone, L. Ozyuzer, J.F. Zasadzinski, P. Romano, D.G. Hinks, C. Kendziora, G.W. Crabtree, and K.E. Gray, Phys. Rev. Lett. **80**, 153 (1998).

[8] N. Miyakawa, P. Guptasarma, J.F. Zasadzinski, D.G. Hinks, and K.E. Gray, Phys. Rev. Lett. **80**, 157 (1998).

[9] A. K. Gupta and K.-W. Ng, Phys. Rev. B **58**, 8901 (1998).

[10] V.J. Emery and S.A. Kivelson, Nature (London) **374**, 434 (1995); M. Randeria, cond-mat/9710223 (unpublished); Q. Chen, I. Kosztin, B. Jankó, and K. Levin, Phys. Rev. Lett. **81**, 4708 (1998).

[11] X.-G. Wen and P.A. Lee, Phys. Rev. Lett. **80**, 2193 (1998).

[12] C.N. Yang and S.-C. Zhang, Mod. Phys. Lett. B **4**, 759 (1990); S.-C. Zhang, Phys. Rev. Lett. **65**, 120 (1990).

[13] S.-C. Zhang, Science **275**, 1089 (1997).

[14] R. S. Markiewicz and M. T. Vaughn, J. Phys. Chem. Solids **59**, 1737 (1998); Phys. Rev. B **57**, 14 052 (1998).

[15] T.M. Rice and G.K. Scott, Phys. Rev. Lett. **35**, 120 (1975).

[16] C. Balseiro and L.M. Falicov, Phys. Rev. B **20**, 4457 (1979).

[17] J.W. Loram, K.A. Mirza, J.R. Cooper, W.Y. Liang, and J.M. Wade, J. Supercond. **7**, 243 (1994).

[18] R.S. Markiewicz, J. Phys. Chem. Solids **58**, 1179 (1997).

[19] B.O. Wells, Z.X. Shen, A. Matsuura, D.M. King, M.A. Kastner, M. Greven, and R.J. Birgeneau, Phys. Rev. Lett. **74**, 964 (1995).

[20] R.B. Laughlin, J. Phys. Chem. Solids **56**, 1627 (1995).

[21] X.-G. Wen and P.A. Lee, Phys. Rev. Lett. **76**, 503 (1996).

[22] R.S. Markiewicz, Phys. Rev. B **56**, 9091 (1997).

[23] I. Affleck and J.B. Marston, Phys. Rev. B **37**, 3774 (1988).

[24] R.S. Markiewicz, J. Phys.: Condens. Matter **2**, 665 (1990).

[25] Earlier references summarized on p. 1223 of Ref. 18; N. Furukawa and T.M. Rice, J. Phys.: Condens. Matter **10**, L381 (1998); N. Furukawa, T.M. Rice, and M. Salmhofer, Phys. Rev. Lett. **81**, 3195 (1998); G. Hildebrand, E. Arrigoni, C. Gröber, and W. Hanke, Phys. Rev. B **59**, 6534 (1999).

[26] J.M. Tranquada, B.J. Sternlieb, J.D. Axe, Y. Nakamura, and S. Uchida, Nature (London) **375**, 561 (1995); J.M. Tranquada, J.D. Axe, N. Ichikawa, A.R. Moodenbaugh, Y. Nakamura, and S. Uchida, Phys. Rev. Lett. **78**, 338 (1997).

[27] H.J. Schulz, Phys. Rev. B **39**, 2940 (1989).

[28] H.-H. Lin, L. Balents, and M.P.A. Fisher, Phys. Rev. B **58**, 1794 (1998).

[29] R.S. Markiewicz, Physica C **193**, 323 (1992).

[30] R.S. Markiewicz, Phys. Rev. Lett. **73**, 1310 (1994).

[31] R.S. Markiewicz and C. Kusko cond-mat/9802079 (unpublished).

[32] J.L. Tallon, J.R. Cooper, P.S.I.P.N. de Silva, G.V.M. Williams, and J.W. Loram, Phys. Rev. Lett. **75**, 4114 (1995); J. W. Loram, J. R. Cooper, K. A. Mirza, N. Athanassopoulou, and W. Y. Liang (unpublished).

[33] J. W. Loram, K. A. Mirza, J. R. Cooper, N. Athanassopoulou, and W. Y. Liang, in *Proceedings of the 10th Anniversary HTS Workshop on Physics, Materials, and Applications*, edited by B. Batlogg, C.W. Chu, W.K. Chu, D.U. Gubser, and K.A. Müller (World Scientific, Singapore, 1996), p. 341.

[34] M. Kiselev, F. Onufrieva, and P. Pfeuty, cond-mat/9804263 (unpublished).

[35] J. W. Loram, K. A. Mirza, J. R. Cooper, and J. L. Tallon, J. Phys. Chem. Solids **59**, 2091 (1998).

[36] Summarized in Secs. 11.4–6 of Ref. 18.

[37] G.S. Boebinger, Y. Ando, A. Passner, T. Kimura, M. Okuya, J. Shimoyama, K. Kishio, K. Tamasaku, N. Ichikawa, and S. Uchida, Phys. Rev. Lett. **77**, 5417 (1996).
[38] J.C. Naeini, X.K. Chen, J.C. Irwin, M. Okuya, T. Kimura, and K. Kishio, Phys. Rev. B **59**, 9642 (1999).
[39] R.S. Markiewicz, Physica C **169**, 63 (1990).
[40] *Dynamical Groups and Spectrum Generating Algebras*, edited by A. Bohm, Y. Ne'eman, and A. O. Barut (Singapore, World Scientific, 1988).
[41] A.I. Solomon and J.L. Birman, J. Math. Phys. **28**, 1526 (1987).
[42] R.S. Markiewicz, Physica C **200**, 65 (1992).
[43] R.S. Markiewicz, Physica C **210**, 235 (1993); **207**, 281 (1993).
[44] G.D. Mahan, *Many Particle Physics*, 2nd ed (Plenum, New York, 1990), Sec. 9.3.
[45] W.A. Harrison, Phys. Rev. **123**, 85 (1961); Z. Yusov, J.F. Zasadzinski, and L. Coffey, cond-mat/9709249 (unpublished).
[46] J.Y.T. Wei, C.C. Tsuei, P.J.M. van Bentum, Q. Xiong, C.W. Chu, and M.K. Wu, Phys. Rev. B **57**, 3650 (1998).
[47] A.A. Varlamov, A.V. Pantsulaya, and M.V. Fistul', Zh. Éksp. Teor. Fiz. **93**, 701 (1987) [Sov. Phys. JETP **66**, 396 (1987)].
[48] A.M. Gabovich, Sov. J. Low Temp. Phys. **18**, 490 (1992).
[49] P.A. Lee, T.M. Rice, and P.W. Anderson, Phys. Rev. Lett. **31**, 462 (1973).
[50] M.V. Sadovskii, Zh. Éksp. Teor. Fiz. **77**, 2070 (1979) [Sov. Phys. JETP **50**, 989 (1979)].
[51] O. Tchernyschov, Phys. Rev. B **59**, 1358 (1999).
[52] D. Coffey and L. Coffey, Phys. Rev. Lett. **70**, 1529 (1993).
[53] H. Ding, Bull. Am. Phys. Soc. **43**, 884 (1998).
[54] H. Ding, J.C. Campuzano, M.R. Norman, M. Randeria, T. Yokoya, T. Takahashi, T. Takeuchi, T. Mochiku, K. Kadowaki, P. Guptasarma, and D.G. Hinks, J. Phys. Chem. Solids **59**, 1888 (1998).
[55] Ch. Renner, B. Revaz, K. Kadowaki, I. Maggio-Aprile, and O. Fischer, Phys. Rev. Lett. **80**, 3606 (1998).
[56] P.J. White, Z.-X. Shen, C. Kim, J.M. Harris, A.G. Loeser, P. Fournier, and A. Kapitulnik, Phys. Rev. B **54**, 15 669 (1996).
[57] B. Batlogg, H.Y. Hwang, H. Takagi, R.J. Cava, H.L. Kao, and J. Kwo, Physica C **235-240**, 130 (1994).
[58] Y.J. Uemura, G.M. Luke, B.J. Sternlieb, J.H. Brewer, J.F. Carolan, W.N. Hardy, R. Kadano, J.R. Kempton, R.F. Kiefl, S.R. Kreitzman, P. Mulhern, T.M. Riseman, D.Ll. Williams, B.X. Yang, S. Uchida, H. Takagi, J. Gopalakrishnan, A.W. Sleight, M.A. Subramanian, C.L. Chien, M.Z. Cieplak, G. Xiao, V.Y. Lee, B.W. Statt, C.E. Stronach, W.J. Kossler, and X.H. Yu, Phys. Rev. Lett. **62**, 2317 (1989).
[59] C. Zhou and H.J. Schulz, Phys. Rev. B **45**, 7397 (1992); F. Wenger and S. Östlund, *ibid.* **47**, 5977 (1993).
[60] R.S. Markiewicz and B.C. Giessen, Physica C **160**, 497 (1989).
[61] M.R. Norman, H. Ding, M. Randeria, J.C. Campuzano, T. Yokoya, T. Takeuchi, T. Takahashi, T. Mochiku, K. Kadowaki, P. Guptasarma, and D.G. Hinks, Nature (London) **392**, 157 (1998).
[62] M.R. Norman, M. Randeria, H. Ding, and J.C. Campuzano, Phys. Rev. B **57**, 11 093 (1998).
[63] V.B. Geshkenbein, L.B. Ioffe, and A.I. Larkin, Phys. Rev. B **55**, 3173 (1997).
[64] A. Nazarenko, J. R. Engelbrecht, and M. Randeria, J. Phys. Chem. Solids **59**, 1745 (1998).
[65] H. Ding, M.R. Norman, T. Yokoya, T. Takeuchi, M. Randeria, J.C. Campuzano, T. Takahashi, T. Mochiku, and K. Kadowaki, Phys. Rev. Lett. **78**, 2628 (1997).
[66] P. Miller, J.K. Freericks, and E.J. Nicol, Phys. Rev. B **58**, 14 498 (1998).
[67] Z.-X. Shen, P.J. White, D.L. Feng, C. Kim, G.D. Gu, H. Ikeda, R. Yoshizaki, and N. Koshizuka, Science **280**, 259 (1998).
[68] A. Kampf and J.R. Schrieffer, Phys. Rev. B **41**, 6399 (1990); **42**, 7967 (1990).
[69] R. A. Klemm (unpublished).
[70] L. Balents, M.P.A. Fisher, and C. Nayak, Int. J. Mod. Phys. B **12**, 1033 (1998).
[71] C.-L. Wu, C.-Y. Mou, X.-G. Wen, and D. Chang, cond-mat/9811146 (unpublished).
[72] C. Kusko, R.M. Markiewicz, and M.T. Vaughn (unpublished).
[73] A. Nazarenko, K.J.E. Vos, S. Haas, E. Dagotto, and R.J. Gooding, J. Supercond. **8**, 671 (1995).
[74] P.G. Radaelli, J.D. Jorgensen, R. Kleb, B.A. Hunter, F.C. Chou, and D.C. Johnston, Phys. Rev. B **49**, 6239 (1994); B.W. Statt, P.C. Hammel, Z. Fisk, S.-W. Cheong, F.C. Chou, D.C. Johnston, and J.E. Schirber, *ibid.* **52**, 15 575 (1995).
[75] W. Ting, O.-M. Nes, T. Suzuki, M.G. Karkut, K. Fossheim, Y. Yaegashi, H. Yamauchi, and S. Tanaka, Phys. Rev. B **48**, 607 (1993).
[76] C. Panagopoulos and T. Xiang, Phys. Rev. Lett. **81**, 2336 (1998).
[77] A. Mourachkine, cond-mat/9810161 (unpublished).
[78] N. Miyakawa, J.F. Zasadzinski, L. Ozyuzer, P. Guptasarma, D.G. Hinks, C. Kendziora, and K.E. Gray, cond-mat/9809398 (unpublished).
[79] R.S. Markiewicz and C. Kusko, cond-mat/9810214 (unpublished).
[80] J. Corson, R. Mallozzi, J. Orenstein, J.N. Eckstein, and I. Bozovic, Nature (London) **398**, 221 (1999).
[81] I.F.G. Parker, M. Endres, P.J. Thomas, G. Yang, A. Yurgens, and C.E. Gough, cond-mat/9809328 (unpublished).
[82] D.K. Morr, Phys. Rev. B **58**, 587 (1998).
[83] Y. Kuroda and C.M. Varma, Phys. Rev. B **42**, 8619 (1990); P.B. Allen and D. Rainer, Nature (London) **349**, 396 (1991); R.S. Markiewicz, Physica C **183**, 303 (1991).